Quantification of the Binding of Insulin-like Growth Factor-I (IGF-I) and IGF Binding Protein-3 (IGFBP-3) Using Surface Plasmon Resonance

Theresa R. Cassino

Thesis submitted to the Faculty of the
Virginia Polytechnic Institute and State University
in partial fulfillment of the requirements for the degree of

Masters of Science
in
Chemical Engineering

Kimberly Forsten-Williams, Chair
Raymond E. Dessy
Kevin E. VanCott

May 30, 2002
Blacksburg, Virginia

Keywords: Insulin-like Growth Factor-I (IGF-I), Insulin-like Growth Factor Binding Protein-3 (IGFBP-3), Surface Plasmon Resonance, Binding Affinity, Biosensor, Growth Factor

Quantification of the Binding of Insulin-like Growth Factor-I (IGF-I) and IGF Binding Protein-3 (IGFBP-3) Using Surface Plasmon Resonance

Theresa R. Cassino

(ABSTRACT)

Insulin-like growth factor-I is a small growth factor known to signal in a variety of mammalian cells through the IGF-I cell surface receptor (IGF-IR). A unique feature of the IGF-I system is the regulation of this binding by soluble IGF binding proteins. Recent studies from our laboratory show that there is a pH dependence in the association of IGF-I with the cell surface in the presence of IGFBP-3 which suggested increased association of IGF-I with IGFBP-3 at low pH. We studied cell free interaction of IGF-I and IGFBP-3 as a function of pH using surface plasmon resonance (SPR) in order to understand the mechanism that causes the increased association. In our studies three different SPR instruments with different surfaces for immobilization of one of the binding partners were used: a Leica Bio-SPR 9000 with a low molecular weight carboxymethylated dextran (CMD) surface, a BIAcore® 2000 with a high molecular weight CMD surface and a Leica SPR 2001 Alpha with a planar mixed self-assembled monolayer (mSAM) surface. Since the experimental system we used was transport sensitive, only the mSAM surface, under optimized conditions, produced results that fit to a single site model. Results suggest that use of CMD layers for immobilization of one partner of a high-affinity binding complex can result in transport limited binding for which simple analysis is inappropriate. Future studies are planned to expand the work with the mSAM surface to elucidate whether a significant difference between the binding parameters as a function of pH exists.

Dedication

This thesis is dedicated to my wonderful husband, Christopher.
Without his constant love and support, I would not be where I am today.

Author's Acknowledgments

First, I would like to acknowledge my advisor, Dr. Kim Forsten-Williams, for her constant support.

Second, to my husband Christopher, a great big thank you for his help with the drawings for this thesis and for moral support throughout the entire process.

To my parents, Mary and Toby Gouker, and my brothers and sisters, Joel, Gina, Danny and Christa Gouker, thanks for all your love and support. Without you all I would not have finished high school, graduated from Rowan and certainly not pursued a graduate degree.

I would also like to acknowledge Dr. Ray Dessy of the Dept. of Chemistry, VPI&SU, for his encouragement and helpful comments. I appreciate all of the time you spend explaining SPR and helping with data analysis and troubleshooting.

To Alexandr Rafailov, a summer REU student for Dr. Forsten-Williams, thank you for your help in troubleshooting countless SPR problems and for running experiments on the Leica Instrument at Virginia Tech.

Acknowledgment also goes to Ky Lowenhaupt, MIT, for her assistance with learning to use the BIAcore 2000 Instrument and helpful discussion about the experimental setup. Thanks also to Dr. Doug Lauffenburger, MIT, for allowing me to have access to the BIAcore instrument and for paying for my hotel room during my time in Boston.

I would like to thank Hans Trutnau, Leica Microsystems Inc., for his helpful discussions about experimental procedures and data analysis. Thanks also to Thor Roalsvig, Leica Microsystems Inc., for his assistance in running the experiments in Buffalo and for interesting conversations about this project.

A special thanks to Thomas Ryan, Leica Microsystems Inc., for all of his help. Tom spent hours analyzing data, troubleshooting and running experiments with me to help obtain meaningful results. He also kindly allowed me to use his laboratory in Buffalo to run a set of experiments. Thank you very much, Tom.

Financial support for this project was from NSF via a grant to Dr. Forsten-Williams (BES-9875626). A GSA graduate research development program grant was also awarded to Theresa Cassino to aid in the completion of this project. I would also like to acknowledge Dr. Bev Watford and the G.E. Scholars program. Without the financial support from this program, I would not have been able to begin my research.

Thanks to Desmond Mascarenhas, Protegen Inc. (Moutainview, California), for his kind gift of the IGFBP-3 used in these experiments.

Thanks also to Christine Campagnola and Dr. Changcheng Zhu of Professor Carl Batts' laboratory at Cornell University in Ithica, NY for preparing the mSAM slides used in our experiment.

Table of Contents

List of Figures

List of Tables

Chapter 1 – Introduction

1.0 Overview of the Chapter

This chapter will provide an introduction to facilitate understanding of the motivation for the studies performed in conjunction with this work. First, a brief overview of the insulin-like growth factor family will be given with particular attention to insulin-like growth factor-I (IGF-I) and insulin-like growth factor binding protein-3 (IGFBP-3). The importance of pH in the biological system and recent studies from Dr. Forsten-Williams' laboratory describing a difference in binding at different pH levels are explained next. Following the explanations of binding differences due to pH levels, the chapter will briefly describe the problem we have investigated in our work. A summary of methods used previously to quantify the interaction of IGF-I and IGFBP-3 will be described next. An overview of the methodology we chose for our experiments, SPR is also given. The chapter concludes with an outline of the rest of the thesis.

1.1 The Insulin-like Growth Factor Family

Members of the insulin-like growth factor family are involved in the regulation of somatic growth and cellular proliferation both in vivo and in vitro (Jones and Clemmons 1995; Ferry, Katz et al. 1999; Collett-Solberg and Cohen 2000). Members of this family include the insulin-like growth factors (IGF-I and IGF-II), insulin-like growth factor binding proteins (IGFBPs) and the IGFBP proteases (Collett-Solberg and Cohen 2000). IGF-I is a small (~ 7.5 kDa) growth factor that is 70 amino acids in length and is capable of signaling a variety of cell activities including cell proliferation (reviewed in Jones and Clemmons 1995; Ferry, Katz et al. 1999; Collett-Solberg and Cohen 2000) and referenced therein), differentiation (Pahlman, Meyerson et al. 1991; Mochizuki, Hakeda et al. 1992; Geduspan and Solursh 1993) and inhibition of apoptosis (Williams, Smith et al. 1990; Rodriguez-Tarduchy, Collins et al. 1992; Muta and Krantz 1993). IGF-I has been found to not only be involved in normal growth, but also in tumor growth, particularly in breast and lung cancers (reviewed in Werner and LeRoith 1996). IGF-I, like many growth factors, signals by activation of a transmembrane tyrosine kinase protein known as the IGF-I cell surface receptor (IGF-IR) (Jones and Clemmons 1995; Collett-Solberg and Cohen 2000). IGF-I, however, does differ from many growth factors in that specific binding proteins known as IGF binding proteins can regulate its bioavailability.

There are six IGFBP that bind IGFs with high affinity and specificity. The major functions of these binding proteins are to 1) prolong the half-life of IGFS in circulation 2) prevent IGF induced hypoglycemia 3) regulate the passage of IGFs from the vasculiture to the extravascular space 4) limit the bioavailability of the IGFs to interact with cell surface receptors 5) enhance IGF actions and 6) affect cellular proliferation and death via IGFBP receptors (Ferry, Katz et al. 1999). The levels and actions of these binding proteins in vivo can be modulated by the IGFBP proteases (Collett-Solberg and Cohen 2000).

The most abundant IGFBP in serum is IGFBP-3 (Clemmons, Busby et al. 1998; Ferry, Katz et al. 1999; Collett-Solberg and Cohen 2000). In serum, most of the IGF-I and IGF-II are found in a complex formed by IGFs, IGFBP-3 and a non-IGF binding glycoprotein known as the acid labile subunit (ALS) (Jones and Clemmons 1995; Ferry, Katz et al. 1999; Collett-Solberg and Cohen 2000). The molecular weight of IGFBP-3 in its nonglycosolated form is 29 kDa. However, IGFBP-3 is found in circulation in its glycosylated form with a molecular weight between 40 and 44 kDa (Collett-Solberg and Cohen 2000). Its primary function in the circulation is thought to be the prolongment of the half-life of IGF-I.

1.2 Interaction of IGF-I and IGFBP-3

At physiologic pH (7.4), IGFBP-3 in solution appears to decrease the stimulatory effects of IGF-I by preventing binding to the receptor (Collett-Solberg and Cohen 2000). For example, IGFBP-3 inhibits IGF-I induced DNA synthesis in human fibroblasts when it is co-incubated with IGF-I in a dose dependent manner (DeMellow and Baxter 1988). IGFBP-3 and IGF-I form a complex that appears to be inactive with regard to stimulating DNA synthesis in this system. This is sometimes called solution sequestration (Figure 1.2-1). In this case, the affinity of IGF for IGFBP-3 in solution is higher that its affinity for the cell surface receptor (IGF-IR) (McCusker, Camacho-Hubner et al. 1990). This is also seen in porcine smooth muscle cells where the addition of IGFBP-3 to the binding assay buffer decreased the cell surface association of ^{125}I-IGF-I (McCusker, Busby et al. 1991). IGFBP-3 appears to reduce the cell surface association by preventing its association with surface binding sites. The authors suggest that the IGFBP-3 may act to limit the access of IGF-I to its receptor thereby inhibiting cell growth.

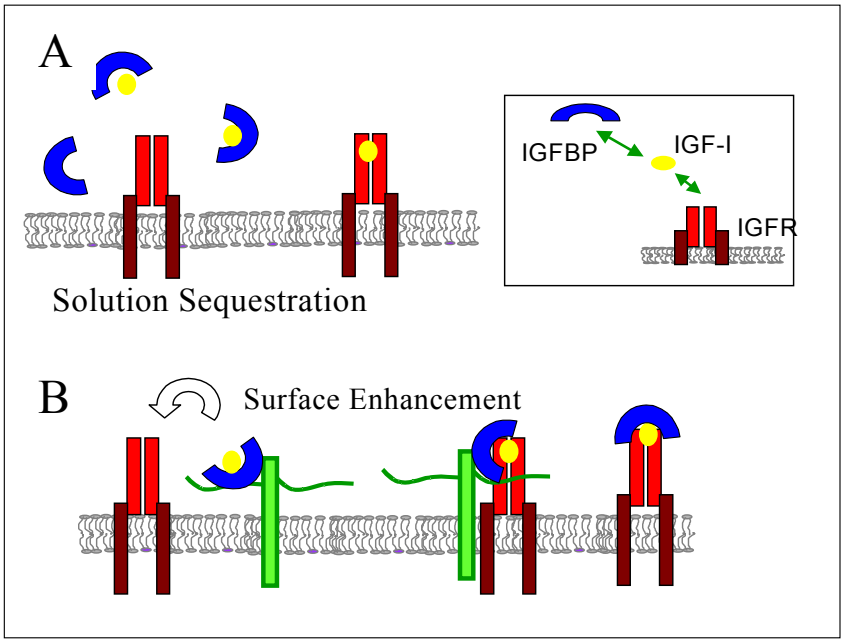

Figure 1.2 -1: Proposed Interactions of IGF-I and IGFBP-3 **A**: Solution Sequestration Model – IGF-I binds to IGFBP-3 preventing its association with IGF-IR **B**: Surface Enhancement Model – IGFBP-3 becomes associated with the cell surface and when IGF-I binds to IGFBP-3 the binding protein encourages interaction of IGF-I and its receptor.

In addition to its action in solution, IGFBP-3 is thought to interact with IGF-I while attached to the cell surface. IGFBP-3 has a glycosaminoglycan binding domain that enables it to bind to the cell surface (Arai, Parker et al. 1994). When IGFBPs adhere to the cell surface, their affinities for IGFs are reduced (McCusker, Camacho-Hubner et al. 1990). This results in an affinity of IGF-I for the surface bound IGFBP-3 similar to its affinity for the IGF-IR. Cell surface bound IGFBP-3 may encourage interaction of IGF-I with the receptor. This is known as surface enhancement (Figure 1.2-1). For example, when bovine fibroblasts are preincubated with IGFBP-3 there is increased responsiveness of the cells to IGF-I in a time-dependent manner which has been attributed to an increase in cell surface associated IGFBP-3 (Conover 1992). These studies suggest that prolonged incubation of fibroblasts with IGFBP-3 has modulatory effects on IGF-IR signal transduction. It should be noted that not all cell-associated IGFBP-3 causes the enhancement of IGF-I action (Karas, Danilenko et al. 1997; Forsten, Akers et al. 2001).

1.3 Importance of pH

Our interest is in studying the effect of pH on the binding of IGF-I with IGFBP-3. Acidification of the extracellular environment is characteristic of most solid tumors (Stubbs, McSheehy et al. 2000), wound sites (Chakkalakal, Mashoof et al. 1994; Spector, Mehrara et al. 2001) and exercised muscle (Street and Juel 2001) suggesting that IGF-I activity could be altered under such conditions. Recent studies from our laboratory have shown pH-dependent binding and trafficking of IGF-I in the presence of IGFBP-3 in mammary epithelial cells (Forsten, Akers et al. 2001). At pH 7.4, the addition of IGFBP-3 decreased the binding of IGF-I to the cell surface when compared to the binding of IGF-I alone while increased binding of IGF-I to the cell surface in the presence of IGFBP-3 over IGF-I alone was seen at pH 5.8. We hypothesize that this difference in cell association of IGF-I is due to increased association of IGF-I with surface bound IGFBP-3. To help determine if the increased cell association was due to increased binding of IGF-I to IGFBP-3, Forsten et al performed a charcoal-binding assay. This experiment showed that binding of ^{125}I-IGF-I to IGFBP-3 was evident at both pH levels, however, approximately three times more binding was seen at pH 5.8 then at pH 7.4 (Forsten, Akers et al. 2001). This result suggested that the binding rate constants at the two pH levels were different. To determine if this hypothesis was correct, the binding rate constants needed to be measured. This work focused on quantitatively measuring the binding rate constants characteristic of IGF-I and IGFBP-3 as a function of pH using surface plasmon resonance (SPR).

1.4 Binding Assays

Several methods have been used to determine binding rate constants in protein systems. Examples of these are charcoal binding (Scott, Martin et al. 1985; Martin and Baxter 1986; Kiefer, Schmid et al. 1992; Oh, Muller et al. 1993; Bach and Rechler 1996), high performance size exclusion chromatography (HPSEC) (Bach and Rechler 1996), polyethylene glycol (PEG) precipitation (McCusker, Busby et al. 1991; Clemmons, Dehoff et al. 1992; Conover 1992), solid-phase assay (Koedam, Hoogerbrugge et al. 1997), immunoprecipitation (Firth, Ganeshprasad et al. 1998), ELISA (Dubaquie and Lowman 1999), calorimetry, filter binding assays, sedimentation equilibrium and fluorescent quenching (Reviewed in Schuck 1997). Charcoal binding (Scott, Martin et al. 1985; Martin and Baxter 1986; Martin, Willetts et al. 1990; Kiefer, Schmid et al. 1992; Oh, Muller et al. 1993; Bach and Rechler 1996), HPSEC (Bach and Rechler 1996), solid-phase assay (Koedam, Hoogerbrugge et al. 1997), immunoprecipitation

(Firth, Ganeshprasad et al. 1998), phage ELISA (Dubaquie and Lowman 1999) and PEG precipitation (McCusker, Busby et al. 1991; Clemmons, Dehoff et al. 1992; Conover 1992) have all been used to quantify the binding between IGFs and IGFBPs and a range of values have been found (Table 1.4-1). Charcoal adsorption assays, PEG precipitation, solid-phase assay and immunoprecipitation require radiolabeling of one of the components for detection. The immunoprecipitation and ELISA assays require the use of antibodies to one of the binding partners.

Table 1.4–1: Binding Measurements for IGF-I Binding to IGFBP-3

Source	Method Used	Binding Parameter	Value
Scott et. al. 1985	Charcoal Adsorption	half maximal displacement	0.16-0.17 ng peptide/0.3 ml assay vol.
Martin and Baxter 1986	Charcoal Adsorption	K_1	$2.1x10^{10}$ M^{-1}
Kiefer et al 1992	Charcoal Adsorption	K_a	$1x10^{10}$ M^{-1}
Oh et al 1993	Charcoal Adsorption	IC_{50}	0.4 ∓ 0.3 ng/ml
McCusker et. al. 1991	PEG Precipitation	K_a	$5.08x10^9$ L/M
Clemmons et. al. 1992	PEG Precipitation	IC_{50}	0.12 nM
Conover 1992	PEG Precipitation	K_a	$1.7x10^{10}$ L/M
Koedam et al 1997	Solid-phase assay	K_D	Saturation 99 ∓ 17 pM Competition 105 ∓ 14 pM
Firth et al 1998	Immunoprecipitation	K_a	152.2 ∓ 33.2 L/nmol
Dubaquie and Lowman 1999	Phage ELISA	IC_{50}	1.01 ∓ 0.42 nM

One problem with the assay techniques that have been previously used for IGF-I binding to IGFBP-3 (charcoal adsorption, PEG precipitation, solid-phase assay, immunoprecipitation, and phage ELISA) is that only equilibrium constants can be obtained. All of these assays require allowing the proteins to come to equilibrium/steady state before measurements are taken. Equilibrium data for several concentrations in the competition experiments are then used in Scatchard plots to obtain the inhibitory concentration of the competitor, IC_{50}, the equilibrium association constant K_A that equals k_a/k_d where k_a is the association rate constant and k_d is the dissociation rate constant or its reciprocal the equilibrium dissociation constant K_D that equals k_d/k_a.

We chose to use SPR for several reasons. First, no labeling of the compounds, either florescent or radiolabeling, is required for detection. SPR also measures the binding progress in

real time allowing for determination of both the association and dissociation constants as opposed to only the ratio of these two that can be determined in equilibrium binding assays. SPR experiments are fairly quick, taking approximately one hour per concentration level. Lastly, SPR has been used previously to measure both the association and dissociation constants for IGFBP-3 and IGF-I. The results from these previous studies will be discussed further in Chapter 2.

1.5 Surface Plasmon Resonance

Surface plasmon resonance is an optical surface sensing technique that can be used to probe refractive index changes that occur within the vicinity of the sensor surface (Earp 1998). The basic SPR optical configuration is referred to as the Kretschmann prism arrangement (Figure 1.5-1). This consists of a prism with a thin metal film, usually gold, coated on one side of it or a

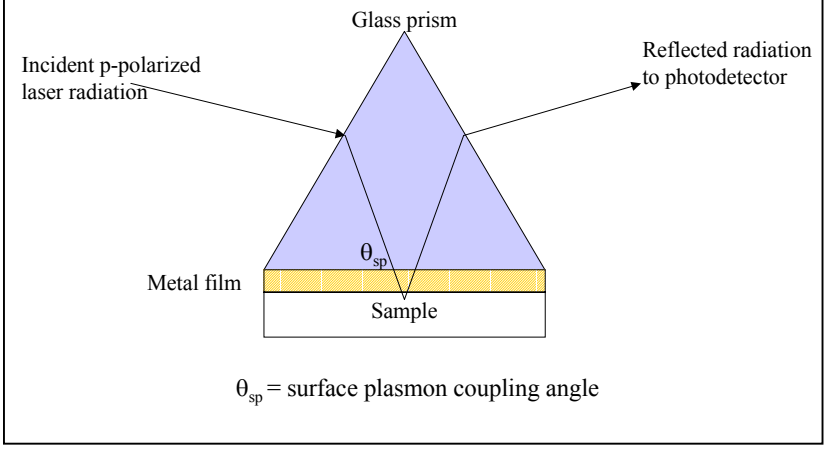

Figure 1.5-1: Kretschmann Prism Arrangement – Redrawn from Earp and Dessy (1998)

metal film deposited on a glass slide that is optically coupled to the prism with refractive index matching fluid (Earp 1998). Total internal reflection of light is used to excite surface plasmons in the metal film (Schuck 1997). Surface plasmons can be described as an oscillation of electrons on the surface of a solid, in this case the thin metal film (Earp 1998). The incoming light is monochromatic and p-polarized (Earp 1998). The light must be p-polarized because only p-polarized light can be coupled into the plasmon mode since this polarization has the electric field oscillating normal to the plane that contains the metal film (Earp 1998). A narrow pass-band optical filter provides a relatively monochromatic light source that assures constant refractive indices of the metal film and the prism (Dessy, Personal Communication). This is

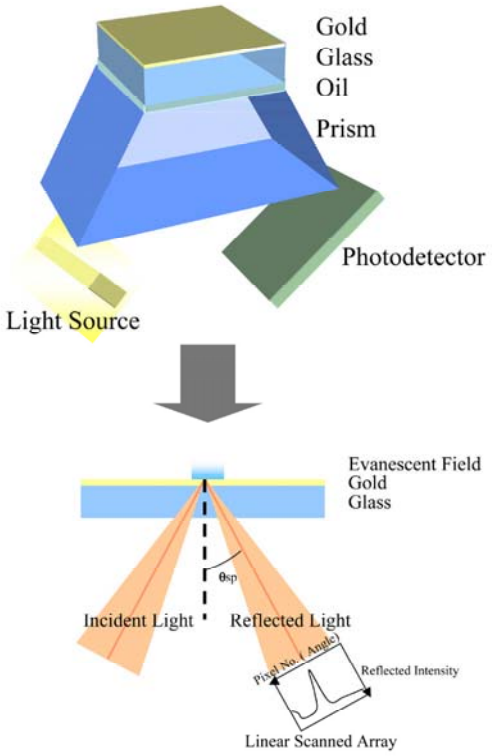

Figure 1.5-2: The Theory Behind Surface Plasmon Resonance
(Used with permission from Leica Microsystems, Inc.)

important because the only variable in the system then is the surface plasmon (SP) coupling angle. Small changes in the refractive index of the sample affect the surface plasmon coupling angle which can be monitored in real time (Earp 1998) (Figure 1.5-2).

In an SPR experiment, one of the binding partners, the ligand, is covalently bound to the surface generally via amine coupling. The other binding partner, the analyte, is flowed over the surface (Earp 1998) (Figure 1.5-3). Binding events at the surface cause a change in refractive index near the sensor surface that changes the SP coupling angle (Schuck 1997). The change in coupling angle is quantitatively detected by the system detector. The detector for all the equipment used in our experiments was a linear array. The detector gives the reflectance minimum caused by the change in coupling angle (Dessy, Personal Communication). This is called the shadowline (Figure 1.5-4). A proprietary super-resolution algorithm was used to find the minimum of the shadowline (Dessy, Personal Communication). These minimums are

measured over time and translated into a binding progress curve or sensorgram. This binding progress curve is expressed in arbitrary units called resonance units (RU) or in pixels and is followed in real time on the computer output screen. The binding progress curve can be fit to an analytical model to determine the binding constants. Analytical models will be described in Chapter 2.

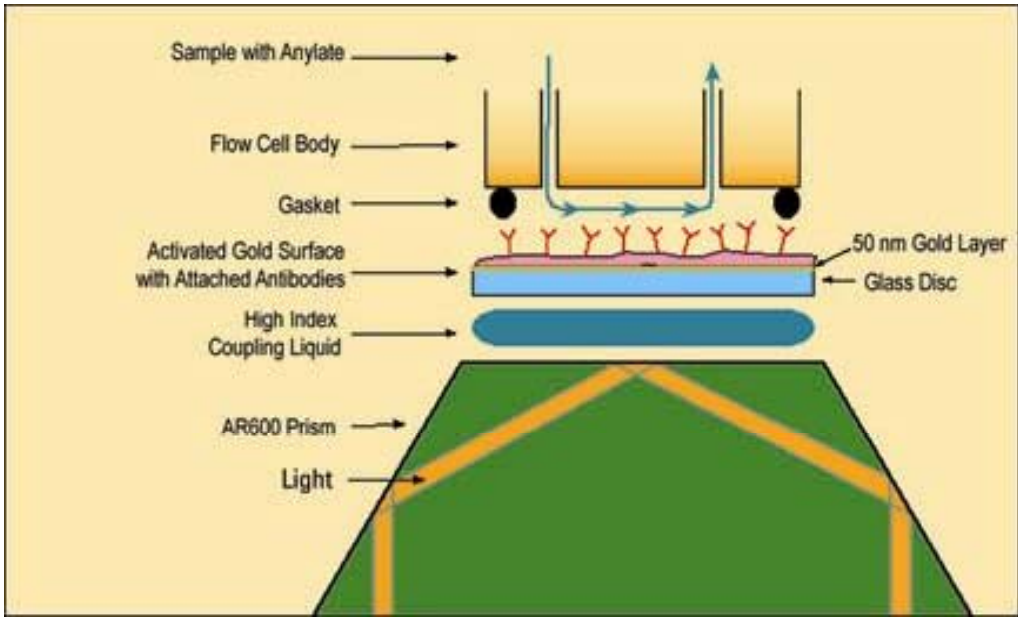

Figure 1.5-3: Flow Cell Schematic (Used with permission from Leica Microsystems Inc.)

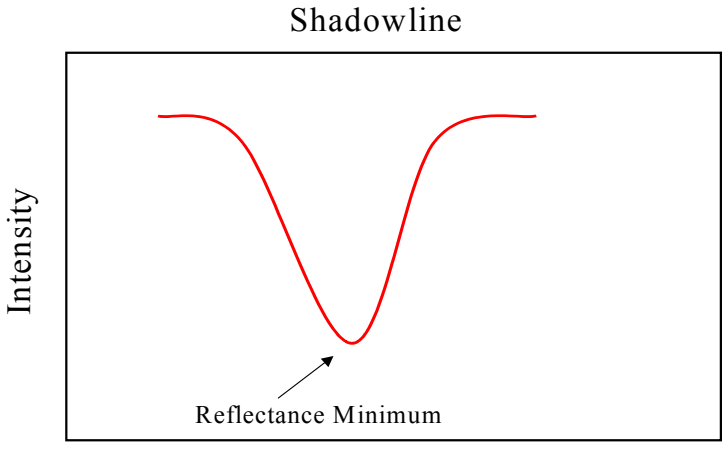

Figure 1.5-4: Shadowline - The Reflectance Minimum Caused by the Change in Coupling Angle

Several different surface types are used to covalently bind the ligand to the surface (Schuck 1997). The surface used for most SPR experiments is a carboxymethyl dextran gel. This type of surface is used because it exhibits low nonspecific adsorption of biomolecules and provides a favorable matrix for biomolecular interactions (Earp 1998). The carboxymethyl dextran (CMD) layer can be converted to amines, hydrazines, maleimides, and sulfhydryls to produce an active surface on which to couple the ligand. The dextran hydrogel surface used for immobilization is approximately 100-150 nm thick. The surface is three-dimensional and relatively thick allowing most of the molecules to be available for interaction after binding to the hydrogel matrix (Figure 1.5-5) (Earp 1998). For our experiments the ligand molecules are immobilized on the sensor surface via amine coupling. This is done by first activating the carboxy groups of the dextran gel with a mixture of N-hydroxysuccinimide (NHS) and N-ethyl-N' (dimethylaminopropyl) carbodiimide to form NHS esters that enable coupling to the amino groups on proteins (Johnsson, Lofas et al. 1991). Protein is then passed over the activated surface and allowed to react attaching primary amine groups to the carboxymethyl dextran layer (Biacore AB 1999). Unreacted NHS esters are hydrolyzed by washing the surface with ethanolamine hydrochloride (Biacore AB 1999) or phosphate buffered saline pH 8.6 (Lahiri, Isaacs et al. 1999).

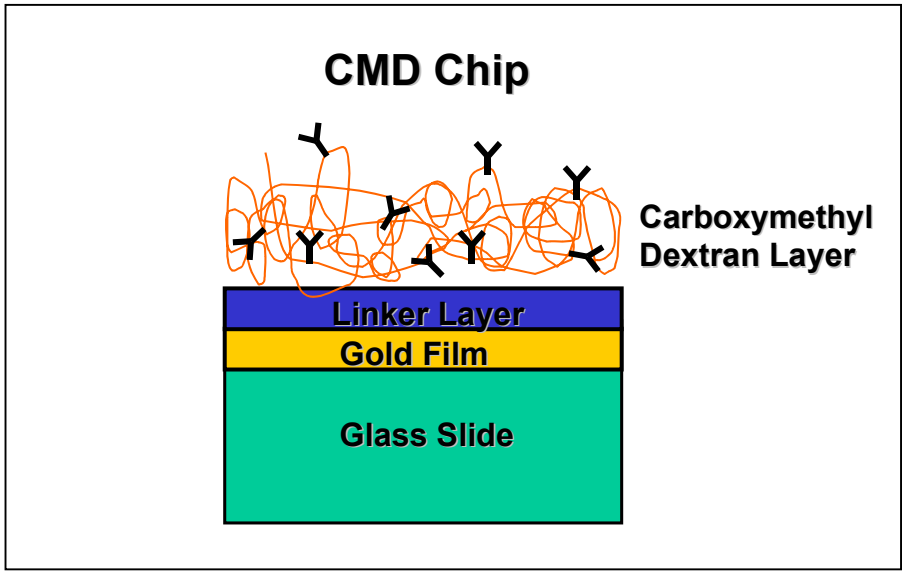

Figure 1.5-5: Schematic of Protein Immobilized to a Carboxymethyl Dextran Surface – The black Y symbols represent the immobilized protein.

While there are benefits to using the dextran gels, the disadvantages of hydrogel matrices make them undesirable for certain applications. Due to the negative charge of the dextran gel nonspecific electrostatic adsorption can be a problem (Schuck 1997; Lahiri, Isaacs et al. 1999). The dextran gel can also cause limits on the diffusion of the analyte to the ligand during association and away from the ligand during dissociation (Schuck 1996; Lahiri, Isaacs et al. 1999; Fong, Wong et al. 2002). To eliminate these issues, the use of a considerably thinner dextran matrix (Schuck 1996), a planar aminosilane derivitized surface (Schuck 1996; Schuck 1997), or a planar self-assembled monolayer surface have been suggested (Schuck 1997; Lahiri, Isaacs et al. 1999; Fong, Wong et al. 2002).

The use of mixed self-assembled monolayers (mSAM) on the gold surface of SPR biosensors has been demonstrated by several researchers (Horan, Yan et al. 1999; Lahiri, Isaacs et al. 1999; Rao, Yan et al. 1999; Fong, Wong et al. 2002). These surfaces have advantages over the carboxymethyl dextran surfaces because they are structurally well characterized, can be tailored to be resistant to nonspecific adsorption and do not have diffusion limitation associated with a dextran layer because the binding occurs at the surface of the SAM (Lahiri, Isaacs et al. 1999; Fong, Wong et al. 2002). Self-assembled monolayer surfaces present a planar configuration for ligand immobilization (Figure 1.5-6). The mixed SAM used for this work contains two compounds; a tri(ethylene glycol)-terminated thiol and a carboxylic acid-terminated thiol. The surface presents free carboxyl groups for amine coupling and polyethylene glycol to minimize non-specific binding (Ryan, Personal Communication). Immobilization of ligand to this surface is achieved by the same procedure as immobilization to the CMD surface described above (Lahiri, Isaacs et al. 1999).

The SPR systems used in this thesis are the Leica Bio-SPR 9000 (Leica Microsystems Inc., Buffalo, NY), the Leica SPR 2001 Alpha (Leica Microsystems Inc., Buffalo, NY) and the BIAcore® 2000 (BIAcore International AB, Uppsala, Sweden). The three systems operate in a similar manner. The major differences are the BIAcore system has an inverted prism system where the immobilized ligands "hang" from the sensor surface and the Leica systems have the prism below with the ligands attached on top of the surface. The BIAcore® system also has a

microfluidics system and robotic control for injection while the Leica systems use manual injection. Specific descriptions of the equipment and operations of each system can be found in Chapters 3 through 5.

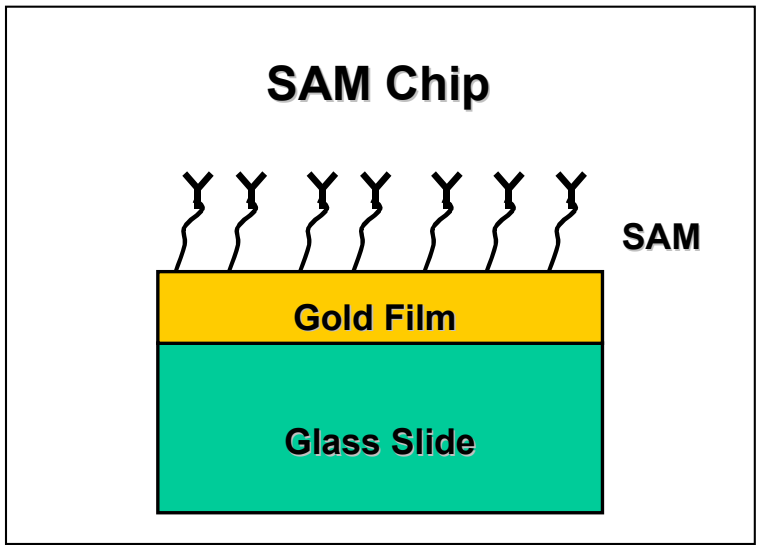

Figure 1.5-6: Schematic of Protein Immobilized to a Self-assembled Monolayer Surface

1.6 Overview of the Thesis

The focus of this thesis is to quantitatively measure the association and dissociation rate constants for the interaction of IGFBP-3 and IGF-I. Our hypothesis is that the binding rate constants will be affected by pH. Specifically, we think that the association and dissociation rate constants will be different at pH 7.4 and pH 5.8. To determine whether this hypothesis is correct, we attempted to quantitatively measure the binding rate constants characteristic of IGF-I and IGFBP-3 as a function of pH using surface plasmon resonance (SPR). It is important to measure the association and dissociation rates separately instead of only measuring the equilibrium constant because the equilibrium constants may be the same although the rate constants are different. The first chapter gave a brief introduction to proteins in the insulin-like growth factor (IGF) family, focusing on IGF-I and IGFBP-3, the importance of studying the effect of pH on binding and the methodology used to study this effect, surface plasmon resonance (SPR). Chapter 2 will review the literature relevant to this study. The most commonly used data analysis methods in SPR detailing the model equations and the SPR work done previously with IGFs and their binding proteins are discussed. The next three chapters describe SPR experiments performed on three different SPR instruments aimed at measuring the

association and dissociation rate constants for IGF-I and IGFBP-3 at pH 7.4 and pH 5.8. Chapter 3 will describe our preliminary studies performed using a Leica Microsystems Inc. Bio-SPR 9000 available at Virginia Polytechnic Institute and State University. It will include a description of the system, experimental procedures, results, data analysis, and conclusions from our specific experiments. The fourth chapter will describe work performed using a BIAcore® 2000 system at the Massachusetts Institute of Technology including a description of the system, experimental procedures, results, data analysis, and conclusions from our experiments. Chapter 5 will describe the experiments performed using a Leica SPR 2001 Alpha at Leica Microsystems Inc. Educational and Analytical Services Division in Buffalo, NY. It will include a description of the system, experimental procedures, results, data analysis, and conclusions from the experiments detailed. Finally, Chapter 6 summarizes the experiments from all three systems and restates the conclusions drawn from all the experiments performed for this thesis. The thesis concludes with suggestions for further studies required to properly characterize this system of proteins.

Chapter 2 – Literature Review

2.0 Overview of the Chapter

This chapter will review current literature relevant to this research. Specifically, this chapter will first discuss literature on data analysis from SPR systems. It will describe in detail the one-site model, the most commonly used model for data analysis in SPR systems, and the modeling equations and assumptions associated it. The two-site and two-compartment models and the conditions under which these models might be useful are also described, as well as the modeling equations and assumptions for these models. Other relevant models are considered briefly. After describing the methods of data analysis generally used with SPR, the results of previous studies performed with SPR using IGFs and IGFBPs are discussed. The chapter specifically describes the proteins used in each experiment, the SPR equipment used, the experimental conditions, the models used to fit the data and results from the experiments. The chapter concludes with a brief summary focusing on IGF-I and IGFBP-3 interaction. This chapter forms the foundation for our research.

2.1 Data Analysis

Data analysis is a key step in SPR studies designed to determine binding affinities for specific protein interactions. Quantification requires that a model be used which (1) accurately reflects the binding interaction and (2) takes into account any transport limitations within the system. Below are described the primary models used for such analysis.

2.1.1 The One-Site Model

2.1.1 – 1 Model Description

The one-site model involves one analyte molecule binding to one immobilized ligand molecule (one to one binding). This model is also known as the rapid mixing model, the simple bimolecular interaction model or 1:1 Langmuir binding model (Pharmacia Biosensor AB 1994; Morton, Myszka et al. 1995; Myszka, He et al. 1998). The one-site model is used to describe most data sets obtained with a SPR biosensor. The major assumptions are that the binding is one to one, the concentration of analyte is constant throughout the flow cell, and the concentration of the analyte does not change with time. Figure 2.1.1-1 shows a schematic of the model system.

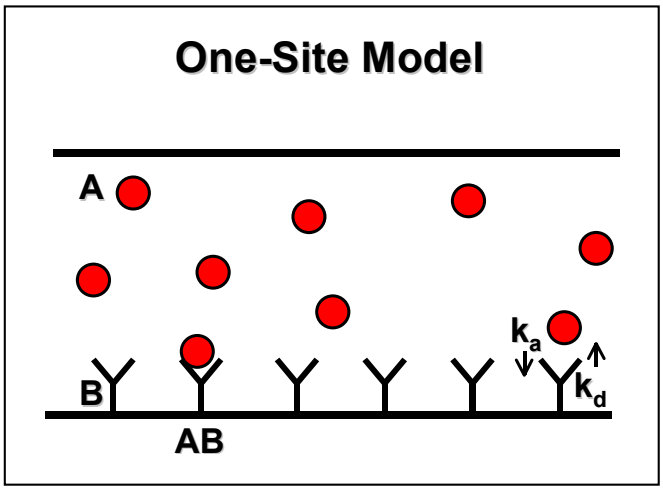

Figure 2.1.1-1: One-Site Model for binding of analyte A to immobilized ligand B to for complex AB – k_a is the association rate constant k_d is the dissociation rate

The model equation and rate equations are shown below (adapted from BIAtechnology Handbook, 1994). The chemical model equation that describes this reaction is

$$A + B \underset{k_d}{\overset{k_a}{\Longleftrightarrow}} AB \qquad \text{Eq. 2.1}$$

where A is the free analyte in solution, B is the ligand immobilized on the sensor surface, AB is the complex of the analyte bound to the ligand, k_a is the association constant and k_d is the dissociation constant. The rate equation for the association phase is

$$\frac{d[AB]}{dt} = k_a[A][B] - k_d[AB] \qquad \text{Eq. 2.2}$$

where d[AB]/dt is the rate of change of the concentration of the complex AB, [A] is the concentration of analyte and [B] is the concentration of unoccupied immobilized ligand. The initial concentration of analyte equals the injection concentration and the initial concentration of the complex AB is zero. The concentration of the unoccupied ligand can be found through equation 2.3

$$[B] = [B]_{\max} - [AB] \qquad \text{Eq. 2.3}$$

where $[B]_{max}$ is the total surface bound ligand and assumes that there is no degradation/inactivation of B on the surface. The rate equation for the dissociation phase is

$$\frac{d[AB]}{dt} = -k_d[AB] \qquad \text{Eq. 2.4}$$

with initial conditions of [AB] at the start of the dissociation phase equals the concentration of AB at the end of the association phase. This is the same equation as the association equation except that it is assumed that [A] is so low throughout the experiment that $k_a[A][B]$ is essentially zero.

Since the response of the instrument, R, is directly related to [AB] the rate equations can be written in terms of response (Pharmacia Biosensor AB 1994). These equations are shown below (Eq. 2.5 and 2.6). For the association phase

$$\frac{dR}{dt} = k_a C R_{\max} - (k_a C + k_d) R \qquad \text{Eq. 2.5}$$

where dR/dt is the rate of change of the SPR signal (response), R_{max} is the maximum analyte binding capacity, and C is the concentration of the analyte. For the dissociation phase

$$\frac{dR}{dt} = -k_d R \qquad \text{Eq. 2.6}$$

Integrating these equations yields

$$R = \frac{k_a C R_{\max}}{k_a C + k_d}\left(1 - e^{-(k_a C + k_d)t}\right) \qquad \text{Eq. 2.7}$$

for the association phase rate equation and

$$\ln\left(\frac{R_1}{R_t}\right) = k_d (t - t_1) \qquad \text{Eq. 2.8 a}$$

or

$$R_t = R_1 e^{-k_d (t - t_1)} \qquad \text{Eq. 2.8 b}$$

for the dissociation phase rate equation where R_t is the response at time t and R_1 is the response at the arbitrary starting time t_1.

2.1.1 – 2 Data Fitting

There are two data fitting methods commonly used for the one-site model, linearization and curve fitting with analytical integration (Morton, Myszka et al. 1995). For linearization of the association data, a plot of dR/dt versus R is made for each concentration of analyte (Pharmacia Biosensor AB 1994). The slope of this plot, s, is equal to $k_a C + k_d$. Next a plot of s versus C, the analyte concentration, is made. The slope of this line is k_a and the intercept is k_d. The dissociation constant, k_d, obtained from this plot is seen as unreliable because a small change in the slope can cause a large change in the k_d value. Due to this unreliability, the dissociation constant is better found via linearization of the data from the dissociation phase of the experiment. This is done by plotting $\ln(R_1/R_t)$ versus $t-t_1$ (Pharmacia Biosensor AB 1994). This plot will give a straight line with the slope equal to k_d and the intercept at zero. Data from all concentrations of the analyte should fall along the same straight line and yield the same dissociation constant.

The second method of data fitting is curve fitting with analytical integration. This method involves fitting the data directly to the nonlinear rate equations (Eq. 2.7 and 2.8 a) (Morton, Myszka et al. 1995). For the association phase of the experiment the data is fit to Equation 2.9

$$R = Y_{\max}\left(1 - e^{-k_{obs}t}\right) \qquad \text{Eq. 2.9}$$

where $Y_{max} = (k_a C R_{max}) / (k_a C + k_d)$ and $k_{obs} = k_a C + k_d$. Plotting k_{obs} versus concentration of analyte, C, yields a straight line with a slope of k_a and an intercept of k_d. Again the k_d value obtained from this plot is seen as unreliable so the dissociation phase data must be used to obtain the dissociation constant. To do this, the data from the dissociation phase is fit directly to Equation 2.8 a and k_d is obtained. The value of the dissociation constant should be the same for all concentrations of the analyte (Pharmacia Biosensor AB 1994).

2.1.2 The Two-Site Model

2.1.2-1 Model Description

The two-site model involves one analyte molecule binding to one immobilized ligand molecule (one to one binding) however, there are two distinct populations of sites for the

immobilized ligand. This model is also known as the surface heterogeneity model (Morton, Myszka et al. 1995). The major assumptions are that there are two different forms of the ligand

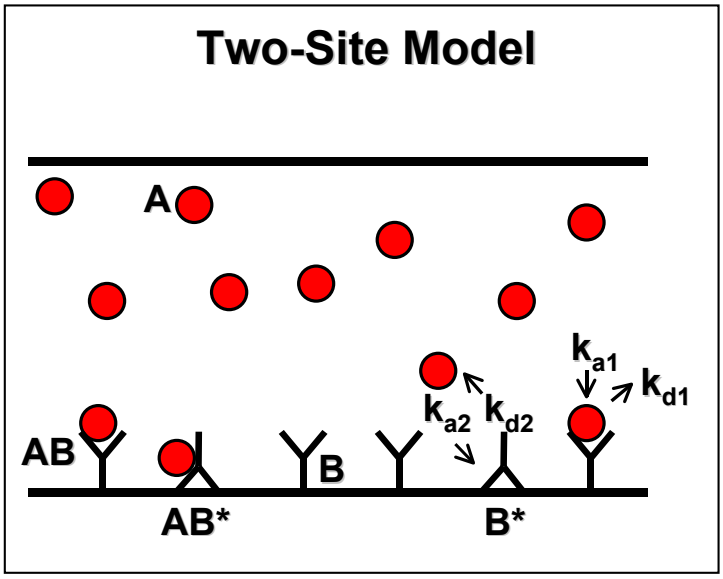

Figure 2.1.2 – 1: Two-Site Model for binding of analyte A to immobilized ligand B or B* to form complex AB or AB*.

immobilized on the sensor surface and each form can bind the analyte in a simple bimolecular interaction (Morton, Myszka et al. 1995). These two different populations of ligand are caused by inhomogeneties in the immobilization of the ligand on the sensor surface that create binding sites with different affinities for the analyte. Each form of the immobilized ligand has different rate constants (Morton, Myszka et al. 1995). Further assumptions are that the concentration of analyte is constant throughout the flow cell and the concentration of the analyte does not change with time. Figure 2.1.2-1 illustrates this model in a simple schematic.

The model equation and rate expressions are shown below (adapted from Heding et al. 1996 and Morton, Myszka et al. 1995). The chemical equations that describe this reaction are

$$A + B \underset{k_{d1}}{\overset{k_{a1}}{\Longleftrightarrow}} AB \qquad \text{Eq. 2.10 a}$$

$$A + B^{*} \underset{k_{d2}}{\overset{k_{a2}}{\Longleftrightarrow}} AB^{*} \qquad \text{Eq. 2.10 b}$$

where B is the ligand of one population immobilized on the sensor surface, B^* is the ligand of the second population immobilized on the sensor surface, AB is the complex of the analyte bound to the ligand of the first population, AB^* is the complex of the analyte bound to the ligand of the second population, k_{a1} and k_{a2} are the association constants and k_{d1} and k_{d2} are the dissociation constants. The rate equations for the association phase are

$$\frac{d[AB]}{dt} = k_{a1}[A][B] - k_{d1}[AB] \qquad \text{Eq. 2.11 a}$$

$$\frac{d[AB^*]}{dt} = k_{a2}[A][B^*] - k_{d2}[AB^*] \qquad \text{Eq. 2.11 b}$$

where d[AB]/dt is the rate of change of the concentration of the complex AB, $d[AB^*]/dt$ is the rate of change of the concentration of the complex AB^*, [B] is the concentration of unoccupied immobilized ligand in the first form and $[B^*]$ is the concentration of unoccupied immobilized ligand in the second form. The unoccupied ligand in the first form can be found by equation 2.12 a and in the second form can be found using equation 2.12b

$$[B] = [B]_{\max} - [AB] \qquad \text{Eq. 2.12 a}$$

$$[B^*] = [B^*]_{\max} - [AB^*] \qquad \text{Eq. 2.12 b}$$

where $[B]_{max}$ is the total surface bound ligand in the first conformation and $[B^*]_{max}$ is the total surface bound ligand in the second conformation. Note that the analyte concentration would be dependent on binding to both B and B^* however A is generally considered a constant. The initial concentration of A is equal to the injection concentration and the initial concentrations of complexes AB and AB* are zero. The rate equations for the dissociation phase are:

$$\frac{d[AB]}{dt} = -k_{d1}[AB] \qquad \text{Eq. 2.13 a}$$

$$\frac{d[AB^*]}{dt} = -k_{d2}[AB^*] \qquad \text{Eq. 2.13 b}$$

where the initial concentration of AB equals the concentration of AB at the end of the association phase and the initial concentration of AB* equals the concentration of AB* at the end of the association phase. The integrated rate equations in terms of response are shown below as:

$$R = \frac{k_{a1} C R_{\max}}{k_{a1} C + k_d} \left(1 - e^{-(k_{a1} C + k_{d1})t}\right) + \frac{k_{a2} C R^*_{\max}}{k_{a2} C + k_{d2}} \left(1 - e^{-(k_{a2} C + k_{d2})t}\right) \quad \text{Eq. 2.14}$$

for the association phase rate equation and

$$R = D_1 e^{-k_{d1} t} + D_2 e^{-k_{d2} t} \quad \text{Eq. 2.15}$$

for the dissociation phase rate equation where D_1 is the response at the start of dissociation for site 1 and D_2 is the response at the start of dissociation for site 2 (Morton, Myszka et al. 1995).

2.1.2-2 Data Fitting

Fitting data to the two-site model is similar to the second method of data fitting for the one-site model, curve fitting with analytical integration. This method involves fitting the data directly to the nonlinear rate equations (Eq. 2.14 and 2.15) (Morton, Myszka et al. 1995). For the association phase of the experiment the data is fit to Equation 2.16

$$R = Y_{\max 1} \left(1 - e^{-k_{obs1} t}\right) + Y_{\max 2} \left(1 - e^{-k_{obs2} t}\right) \quad \text{Eq. 2.16}$$

where $Y_{max1} = (k_{a1}\, C\, R_{max1}) / (k_{a1}\, C + k_{d1})$, $k_{obs1} = k_{a1}\, C + k_{d1}$, $Y_{max2} = (k_{a2}\, C\, R_{max2}) / (k_{a2}\, C + k_{d2})$, $k_{obs2} = k_{a2}\, C + k_{d2}$. Plotting k_{obs1} versus concentration of analyte, C, yields a straight line with a slope of k_{a1} and an intercept of k_{d1}. Similarly plotting k_{obs2} versus concentration of analyte, C, yields a straight line with a slope of k_{a2} and an intercept of k_{d2}. For reasons similar to those in the one-site model, the k_d values obtained from these plots are thought to be unreliable (Pharmacia Biosensor AB 1994). Therefore, the dissociation phase data should be used to obtain the dissociation constants. To do this, the data from the dissociation phase is fit directly to equation 2.15 and k_{d1} and k_{d2} are obtained. The values of the dissociation constants should be the same for all concentrations of the analyte (Pharmacia Biosensor AB 1994).

2.1.3 The Two-Compartment Model

2.1.3-1 Model Description

The two-compartment model is similar to the one-site model in that one assumes a one to one binding between the analyte and the immobilized ligand. However, this model differs from the one-site model in that the concentration of analyte in the flow cell is not constant. There are two compartments that have different analyte concentrations. The bulk compartment has a concentration that equals the injection concentration of the analyte while the surface compartment concentration is determined by the rate of mass transport of the analyte from the bulk solution and binding to the immobilized ligand. The major assumptions are the transport rate only depends on the concentration difference and a concentration-independent rate constant, there is no degradation or inactivation of the proteins during the experiment, there is a constant concentration of A in the bulk compartment, the surface compartment is well mixed. Initial conditions are that in the association phase the concentration of analyte in the bulk compartment is equal to the injection concentration at time equals zero and the concentrations of analyte in the surface compartment and the complex both equal zero at time equals zero. Initial conditions for the dissociation equations are that at the beginning of dissociation the concentration of analyte in the bulk compartment equals zero and the concentrations of analyte and complex in the surface compartment are equal to their concentrations at the end of the association phase. This model is illustrated in Figure 2.1.3-1.

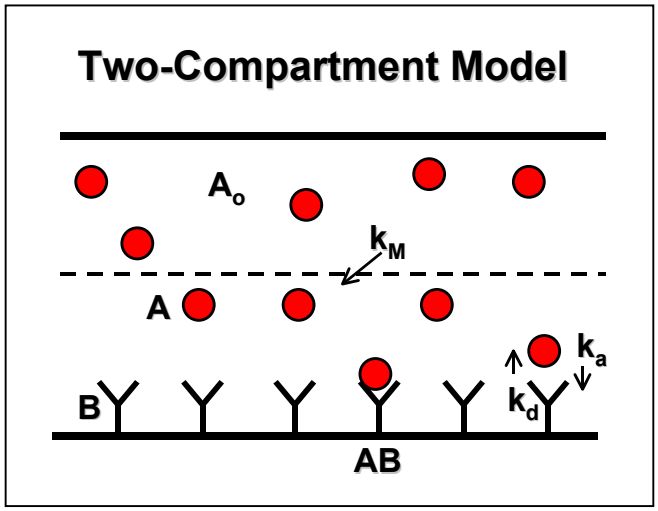

Figure 2.1.3-1: Two-Compartment Model for transport of analyte Ao to the surface (A) and binding of analyte A to immobilized ligand B to form complex AB (adapted from Myszka, He et al.1998)

The model equation and rate equations are shown below (adapted from Myszka, He et al. 1998). The chemical model equation that describes this reaction is

$$A_o \xrightarrow{k_M} A + B \underset{k_d}{\overset{k_a}{\Longleftrightarrow}} AB \qquad \text{Eq. 2.17}$$

where A_o is the free analyte in the bulk compartment, A is the free analyte in the surface, and k_M is the transport coefficient. The rate equations for this model are

$$V_i \frac{d[A]}{dt} = S\left(-k_a[A][B] + k_d[AB] + k_M\left([A_o] - [A]\right)\right) \qquad \text{Eq. 2.18}$$

$$\frac{d[AB]}{dt} = k_a[A][B] - k_d[AB] \qquad \text{Eq. 2.19}$$

where V_i is the volume of the surface compartment, d[A]/dt is the rate of change of the concentration of the analyte A in the surface compartment, and S is the surface area of the flow cell. The unoccupied ligand concentration [B] can be found using Equation 2.20

$$[B] = [B]_{\max} - [AB] \qquad \text{Eq. 2.20}$$

where $[B]_{max}$ is the total surface bound ligand.

2.1.3-2 Data Fitting

Analytical integration of the rate equations for the two-compartment model is difficult. Due to this difficulty, numerical integration of the rate equations is preferable. Myszka and Morton (Morton and Myszka 1998) have developed a numerical non-linear least-squares fitting algorithm to solve Equations 2.18 and 2.19. This algorithm is used in their software program, CLAMP, which is freely available on their website (Morton and Myszka 1998; Myszka, He et al. 1998). This program uses global fitting to fit the association and dissociation data simultaneously for all concentrations of analyte (Myszka, He et al. 1998). A numerical method for solving these equations is also used in the BIAevaluation™ software available from Pharmacia Biosensor (Uppsala, Sweden) (Fong, Wong et al. 2002).

2.1.4 Other Binding Models

Other kinetic models have also been used in SPR studies. These models are generally used for more complex protein-protein interactions. For example, models have been developed which include a two-state conformation change (Morton, Myszka et al. 1995), two-site binding with mass transport (Fong, Wong et al. 2002), second-order kinetics (Edwards, Maule et al. 1998), and a mass transport model incorporating the effects of the dextran layer (Schuck 1996). These models are described elsewhere (Morton, Myszka et al. 1995; Schuck 1996; Edwards, Maule et al. 1998; Fong, Wong et al. 2002) and are not detailed here since we do not believe they are applicable to the protein system investigated in this work.

2.2 Review of Previous SPR Studies Using Insulin-like Growth Factors and Insulin-like Growth Factor Binding Proteins

In this section, descriptions of 8 papers including details related to the experimental conditions and the rate constants obtained from the experiments are presented. The review of each paper contains information about the equipment used, the proteins used, the amount of ligand immobilized, the concentrations of analyte used, the model selected for data fitting and the rate constants obtained from the chosen fitting method. The papers are presented in chronological order.

2.2.1 Heding, Gill, Ogawa, DeMeyts, and Shymok (1996)

The goal of this paper was to study the binding of IGF-I and IGF-I analogues to IGFBP-3. The proteins used in this study were IGF-I, IGF-II, IGF analogues, and IGFBP-3. The authors used an unspecified BIAcore Instrument to make kinetic measurements of the binding of these proteins. All measurements were made at 25 °C. IGFBP-3 was used as the immobilized ligand. For immobilization 10 μl of IGFBP-3 was injected at a concentration of 11 μg/ml and a flow rate of 5 μl/min over the activated surface and covalently bound to the carboxymethyl dextran layer via amine coupling. This resulted in 650 RU of protein immobilized on the CM5 chip. For kinetic measurements IGF-I, IGF-II and IGF analogues were used as analytes. For each analyte 32 μl of 50 nM concentration solution was injected over the immobilized ligand at a flow rate of 8 μl/min. The two-site interaction model was used for fitting the association and dissociation data. The authors chose this model because “the curves were biphasic”. The

parameter for the low affinity site had high variability and could not be determined reliably from these experiments. The authors use the high affinity component as a representation of the specific binding because the low affinity site accounted for less than 10% of total bound ligand. Table 2.2.1-1 shows the kinetic parameters obtained in these experiments for IGF-I, IGF-II and Insulin.

Table 2.2.1-1: Kinetic Constants from Heding et al.

Analyte	**k_a x 10^4 ∓ S.E. (s^{-1} nM^{-1})**	**k_d x 10^4 ∓ S.E. (s^{-1})**	**K_d x 10^4 ∓ S.E. (nM)**
IGF-I	3.5 ∓ 0.37	0.78 ∓ 0.11	0.23 ∓ 0.04
IGF-II	5.2 ∓ 0.74	0.62 ∓ 0.005	0.12 ∓ 0.02
Insulin	0.04 ∓ 0.008	9.5 ∓ 2.8	251 ∓ 91

The authors concluded that IGFBP-3 has a comparable affinity for IGF-I and IGF-II with a slight preference for IGF-II. Insulin was also found to have a small affinity for IGFBP-3 even though the authors did not expect binding of insulin to IGFBP-3.

2.2.2 Jansson, Dixelius, Uhlen and Nilsson (1997)

Jansson et al used IGF-I, IGF-I fusion proteins, IGFBP-1 and the IGF-I receptor as the proteins of interest in this study. An unspecified BIAcore Instrument was used to make kinetic measurements. For the experiments, 50 mg/ml solutions of IGFBP-1 or IGF-IR were immobilized at a flow rate of 5 µl/min and a temperature 25°C on separate CM5 sensor chips. This resulted in 700-2000 RU of immobilized ligand. For the binding experiments, five concentrations of IGF-I, Z-IGF-I or IGF-I-Z (327, 109, 54.5, 27.3 and 13.6 nM) were flowed over the surface. The authors do not list the flow rate used however they state that the association phase was run for 300 seconds. The Z-IGF-I and IGF-I-Z are fusion proteins of the Z protein on either the N or C terminus of IGF-I. The one-site binding model was used to fit the data in this study. Fitting with this model resulted in an association constant of $k_a = 6.1 \times 10^{-5}$ M^{-1} s^{-1}, a dissociation constant of $k_d = 3.5 \times 10^4$ s^{-1} and an equilibrium affinity constant of $K_A = 1.7 \times 10^{-9}$ M^{-1} for IGF-I binding to immobilized IGFBP-1. For IGF-I binding to IGF-IR the association constant was $k_a = 4.7 \times 10^{-5}$ M^{-1} s^{-1}, the dissociation constant was $k_d = 16.7 \times 10^4$ s^{-1}

and the equilibrium affinity constant was $K_A = 0.28 \times 10^{-9}\ M^{-1}$. The results of this study show a difference in the affinity of IGF-I for IGFBP-1 and the affinity of IGF-I for its receptor.

2.2.3 Marinaro, Jamieson, Hogarth, and Bach (1999)

In this paper, the authors studied the interaction of IGFBP-6 (glycosylated and non-glycosylated) with IGF-I and IGF-II using a BIAcore 2000 SPR biosensor. The glycosylated (g-IGFBP-6) or non-glycosylated (ng-IGFBP-6) forms of IGFBP-6 (10 μg/ml) were immobilized on separate activated CM 5 sensor surfaces at a 10 μl/min flow rate and a temperature of 20 °C. This resulted in 682 RU g-IGFBP-6 immobilized and 1642 ng-IGFBP-6 immobilized. For kinetic measurements with IGF-I, concentrations of 1.31, 2.61, 6.54, 13.1, 26.1, 52.3, 105 and 131 nM were used and, for IGF-II, concentrations 1.34, 2.68, 6.69, 13.4, 26.8, 53.5, 107 and 134 nM were used. All kinetic measurements were performed at a flow rate of 10 μl/min. The authors chose to use the two-site model to fit the data from the kinetic experiments. The results for g-IGFBP-6 are shown in table 2.2.3-1 and for ng-IGFBP-6 in table 2.2.3-2. In the tables K_A is the weighted average of the association constants divided by k_{off1}. Each of the association constants is weighted by its relative contributions to the total binding. Only the dissociation constant for the first site was used since the contribution of the second dissociation rate constant was less than 15%.

Table 2.2.3-1: Kinetic Constants for Glycosylated IGFBP-6 from Marinaro et al.

Analyte	$k_{on1} \times 10^5 \mp$ S.E. ($s^{-1}\ M^{-1}$)	$k_{on2} \times 10^5 \mp$ S.E. ($s^{-1}\ M^{-1}$)	$k_{off1} \times 10^{-3} \mp$ S.E. (s^{-1})	$k_{off2} \times 10^{-3} \mp$ S.E. (s^{-1})	$K_A \mp$ S.E. (nM^{-1})
IGF-I	8.9 ∓ 1.32	0.30 ∓ 0.04	20.3 ∓ 0.8	1.1 ∓ 0.1	0.028 ∓ 0.003
IGF-II	9.3 ∓ 0.4	0.31 ∓ 0.00	0.34 ∓ 0.01	11.6 ∓ 0.1	1.88 ∓ 0.16

Table 2.2.3-2: Kinetic Constants for Non-Glycosylated IGFBP-6 from Marinaro et al.

Analyte	$k_{on1} \times 10^5 \mp$ S.E. ($s^{-1}\ M^{-1}$)	$k_{on2} \times 10^5 \mp$ S.E. ($s^{-1}\ M^{-1}$)	$k_{off1} \times 10^{-3} \mp$ S.E. (s^{-1})	$k_{off2} \times 10^{-3} \mp$ S.E. (s^{-1})	$K_A \mp$ S.E. (nM^{-1})
IGF-I	6.5 ∓ 0.1	0.31 ∓ 0.03	19.7 ∓ 0.0	1.3 ∓ 0.1	0.023 ∓ 0.001
IGF-II	2.8 ∓ 0.0	0.18 ∓ 0.00	0.36 ∓ 0.01	10.6 ∓ 0.1	0.55 ∓ 0.01

The authors concluded that IGFBP-6 binds IGF-II preferentially over IGF-I and that glycosylation of IGFBP-6 was found to modestly increase the association kinetics without changing the dissociation kinetics.

2.2.4 Wong, Fong and Yang (1999)

The proteins used in this study were IGF-I, IGF-II, IGFBP-1, IGFBP-2, IGFBP-3, IGFBP-4, IGFBP-5, and IGFBP-6. For these SPR studies, the authors used a BIAcore X SPR biosensor to perform kinetic measurements. Either IGF-I or IGF-II was immobilized on a CM5 sensor chip and the IGF binding proteins were used as analytes. For immobilization, 35 μl of IGF-I or IGF-II at a concentration of 10 μg/ml and a flow rate of 5 μl/min was injected over the activated sensor surface and immobilized via amine coupling. The authors did not indicate how much IGF-I or IGF-II was immobilized on the surface. The temperature of the experiments was 25 °C. Five concentrations (5, 25, 50, 100, and 250 nM) of each binding protein were injected separately over the surface. Each injection was of 32 μl of analyte solution at a flow rate 8 μl/min and a temperature of 25 °C. The authors used the one-site, two-site, two-compartment (one-site with mass transport), one-site with conformational change and competition models to fit the data from the experiments. For all data sets, the one site model was determined to be the best using the chi-squared goodness of fit statistic. Table 2.2.4-1 shows the rate constants for immobilized IGF-I binding to each binding protein. Table 2.2.4-2 shows the rate constants for IGF-II.

Table 2.2.4-1: Kinetic Constants for IGF-I from Wong et al.

Analyte	**k_a x 10^5 ∓ S.E. (s^{-1} M^{-1})**	**k_d x 10^{-5} ∓ S.E. (s^{-1})**	**K_A x 10^9 ∓ S.E. (M^{-1})**
hIGFBP-1	0.11 ∓ 0.02	1.5 ∓ 0.05	0.72 ∓ 0.17
IGFBP-1	0.12 ∓ 0.01	0.97 ∓ 0.02	1.23 ∓ 0.27
IGFBP-2	0.55 ∓ 0.12	2.48 ∓ 0.09	2.28 ∓ 0.45
IGFBP-3	9.12 ∓ 1.65	5.32 ∓ 0.15	18.4 ∓ 3.08
IGFBP-4	2.15 ∓ 0.29	5.60 ∓ 0.16	3.90 ∓ 0.60
IGFBP-5	5.82 ∓ 1.03	10.4 ∓ 0.54	5.68 ∓ 1.10
IGFBP-6	3.02 ∓ 0.36	20.5 ∓ 0.338	1.64 ∓ 0.17

Table 2.2.4-2: Kinetic Constants for IGF-II from Wong et al.

Analyte	k_a x 10^5 ∓ S.E. (s^{-1} M^{-1})	k_d x 10^{-5} ∓ S.E. (s^{-1})	K_A x 10^9 ∓ S.E. (M^{-1})
hIGFBP-1	0.07 ∓ 0.01	3.64 ∓ 0.60	0.21 ∓ 0.05
IGFBP-1	0.32 ∓ 0.04	1.32 ∓ 0.24	2.42 ∓ 0.36
IGFBP-2	1.04 ∓ 0.22	11.4 ∓ 4.83	0.91 ∓ 0.07
IGFBP-3	17.0 ∓ 3.79	3.85 ∓ 0.33	46.5 ∓ 10.0
IGFBP-4	2.20 ∓ 0.64	7.76 ∓ 0.59	2.60 ∓ 0.63
IGFBP-5	12.1 ∓ 1.34	37.4 ∓ 1.76	3.30 ∓ 0.36
IGFBP-6	3.26 ∓ 0.71	21.8 ∓ 0.09	1.50 ∓ 0.33

The authors concluded that all of the binding proteins have similar affinities for IGF-I and IGF-II. The authors compared these results with published literature values for the equilibrium affinity constant, K_A, and concluded that the constants determined by the SPR biosensor were more precise than the values from literature due to smaller errors from the SPR studies. The authors also noted that protein-protein interactions at a solid surface are significantly different than interactions in solution so it is difficult to make a quantitative ranking between different binding assays.

2.2.5 Dubaquie and Lowman (1999)

Dubaquie and Lowman studied the interaction of IGF-I and IGF-I mutants with IGFBP-I and IGFBP-3 in this paper using a BIAcore 2000 instrument. For the kinetic measurements on the BIAcore 2000 instrument, the authors immobilized IGF-I and IGF-I mutants (50 μg/ml concentration) on activated CM5 sensor chips. The immobilization resulted in 400-600 RU of IGF-I or IGF-I mutant on the surface. IGFBP-1 and IGFBP-3 were used as analytes. The flow rate for the kinetic measurements was 20 μl/min and the temperature was 25 °C. Concentrations of 1 μM, 500 nM and 250 nM of each binding protein were run over the different surfaces. The one-site binding model was used to ascertain the kinetic rate constants. The results for immobilized IGF-I are shown in Table 2.2.5-1.

IGFBP-3 was found to have a greater affinity for IGF-I than IGFBP-1 with the difference in affinity resulting from a 10-fold faster association rate. The authors also used a phage display assay to determine the binding affinities between the proteins and the kinetic constants obtained using SPR compared well to the results from the phage display.

Table 2.2.5-1: Kinetic Constants from Dubaquie and Lowman

Analyte	**k_a x 10^5 ∓ S.E. (s^{-1} M^{-1})**	**k_d x 10^{-4} ∓ S.E. (s^{-1})**	**K_D ∓ S.E. (nM^{-1})**
IGFBP-1	32.0 ∓ 2.0	4.1 ∓ 0.2	13.0 ∓ 1.0
IGFBP-3	3.2 ∓ 0.5	4.7 ∓ 0.8	1.5 ∓ 0.3

2.2.6 Galanis, Firth, Bond, Nathanielsz, Kortt, Hudson, and Baxter (2001)

The proteins used for the studies of Galanis et al were IGF-I, IGF-II, IGFBP-3, and fragments of IGFBP-3. An undisclosed BIAcore instrument was used for the SPR kinetic measurements. IGF-I or IGF-II was immobilized using a 20 μg/ml concentration solution at a flow rate of 5 μl/min and a temperature of 25 °C on separate activated CM5 sensor chips. This resulted in 625 RU of immobilized IGF-I and 277 RU of immobilized IGF-II. For measurement of the kinetic parameters, IGFBP-3 or IGFBP-3 fragments (30-50 μl) were injected over the immobilized growth factor at a flow rate of 5 μl/min. To fit the experimental data the authors chose to use the one-site binding model to obtain kinetic rate constants. Fitting of the data for IGFBP-3 injection over IGF-I resulted in an association constant of $k_a = 1.1 \times 10^{-5}$ M^{-1} s^{-1}, a dissociation constant of $k_d \geq 1.0 \times 10^{-6}$ s^{-1} and an equilibrium affinity constant of $K_A \approx 1 \times 10^{11}$ M^{-1}. The authors noted that this interaction was characterized by a very slow dissociation rate.

2.2.7 C.C. Fong, M.S. Wong, W.F. Fong and M. Yang (2002)

The authors used IGF-I, IGFBP-1 and IGFBP-3 as an interaction system in this experiment to help determine the differences between the kinetic constants obtained using a carboxymethyl dextran (CM5) surface and the kinetic constants obtained using a self-assembled monolayer (SAM) surface. The kinetic measurements were made using a BIAcore X instrument. For the CM5 surface, IGF-I, IGFBP-1, or IGFBP-3 was immobilized on the surface via amine

coupling by injecting 35 µl of protein at a concentration 10 µg/ml with a flow rate of 5 µl/min and a temperature of 25°C. For the SAM surface, IGF-I was immobilized by injecting 35 µl of protein at a concentration of 10 µg/ml, a 5 µl/min flow rate and a temperature of 25 °C. To determine the kinetic constants, 32 µl of analyte was injected at a flow rate of 8 µl/min and a temperature of 25 °C. The concentrations of IGF-I over the CM5 surface with either IGFBP-1 or 3 immobilized were 250, 100, 50 and 25 nM. The IGFBP-1 concentrations over the CM5 were 500, 250, 100 and 50 nM and for IGFBP-3 the concentrations were 50, 25, 10 and 5 nM. For IGFBP-1 over the SAM concentrations of 250, 100, 50 and 25 nM were used. The authors indicate that the data fit best to a one-site binding model based on chi-squared statistical comparison with the two-compartment, two-site binding and two-site binding with mass transport models. Results from the experiments are shown in Table 2.2.7-1

Table 2.2.7-1: Kinetic Constants from Fong et al.

Surface	Analyte	Ligand	k_a x 10^5 ∓ S.E. (s^{-1} M^{-1})	k_d x 10^{-4} ∓ S.E. (s^{-1})	K_A x 10^8 ∓ S.E. (M^{-1})
CM5	**IGFBP-1**	**IGF-I**	0.16 ∓ 0.01	8.12 ∓ 0.12	0.20 ∓ 0.01
CM5	**IGF-I**	**IGFBP-1**	7.83 ∓ 0.06	4.81 ∓ 0.17	16.3 ∓ 0.59
CM5	**IGFBP-3**	**IGF-I**	0.73 ∓ 0.02	4.04 ∓ 0.75	1.81 ∓ 0.34
CM5	**IGF-I**	**IGFBP-3**	21.6 ∓ 0.56	7.26 ∓ 0.19	29.8 ∓ 1.09
SAM	**IGFBP-1**	**IGF-I**	3.15 ∓ 0.17	15.9 ∓ 0.44	1.98 ∓ 0.12

The major result of this paper was a difference in the binding over the CM5 surface depending on which binding partner is immobilized. The SAM surface experiment yielded different binding constants than the same protein system on the CM5 surface which the authors concluded may be due to steric effects and limits on analyte diffusion caused by the CMD chip.

2.2.8 Vorwerk, Hohmann, Oh, Rosenfeld and Shymok (2002)

The purpose of this study was to measure the binding of IGF-I and IGF-II to IGFBP-3, an N-terminal IGFBP-3 fragment and a C-terminal IGFBP-3 fragment. IGF-I, IGF-II, IGFBP-3, IGFBP-3 fragments, and Insulin were used for these experiments. Structurally related proteins mac25 and connective tissue growth factor were also studied. The kinetic measurements were made using a BIAcore 1000 instrument with IGFBP-3, IGFBP-3 fragments, IGF-I or IGF-II immobilized on the CM5 sensor chip via amine coupling. A temperature of 25 °C and a flow rate of 5 µl/min were used for immobilization**.** The concentration of protein and immobilization

time for each protein are as follows: IGFBP-3 at 10 μg/ml for 7 minutes, IGF-I at 4 μg/ml for 7 minutes and IGF-II at 1 μg/ml for 7 minutes. The authors indicate that 412 RU of IGFBP-3 was immobilized and 256 RU of IGF-I was immobilized. For the kinetic experiments a constant flow rate of 50 μl/min and a temperature of 25 °C was used. Concentrations of analyte were not given however the authors state that a series of varying concentrations of analyte was used for the kinetic assays. The data was fit using BIAEvaluation 3.0 assuming a one-site model. Kinetic rate constants and equilibrium affinity constants for IGF-I and IGF-II binding to IGFBP-3 are given in Table 2.2.8-1.

Table 2.2.8-1: Kinetic Constants from Vorwerk et al

Analyte	**k_a x 10^5 ∓ S.E. (s^{-1} M^{-1})**	**k_d x 10^{-4} ∓ S.E. (s^{-1})**	**K_A x 10^9 ∓ S.E. (M^{-1})**
IGF-I	7.87 ∓ 1.00	2.09 ∓ 0.35	4.13 ∓ 0.71
IGF-II	7.63 ∓ 1.60	1.78 ∓ 0.53	4.68 ∓ 0.83

The authors compare the values they obtained with the results from studies by Heding, Gill et al. (1996), Wong, Fong et al. (1999) and Galanis, Firth et al. (2001) described earlier in this chapter (Sections 2.2.1, 2.2.4 and 2.2.6). The values obtained in this study differ from the values in the previous studies. The authors attribute these differences to their use of a higher flow rate reducing possible mass transport and rebinding effects and to their use of a global analysis as opposed to fitting each concentration individually. Insulin was found to bind weakly to IGFBP-3 in some of the experiments in this paper but found not to bind in other experiments. The authors state that this indicates that insulin binds IGFBP-3 with low affinity. The authors show that IGF-I and IGF-II bind IGFBP-3 with similar binding kinetics and the affinities of IGF-I and IGF-II for IGFBP-3 fragments are less than their affinities for IGFBP-3.

2.3 Summary

Three data analysis models are described in detail in this chapter: the one-site, the two-site and the two-compartment model. The models described here will be used for the analysis of our experimental data. This description of models for data analysis gives a basic background for the data analysis sections of the next three chapters (Chapters 3, 4 and 5).

The review of pertinent literature in this chapter gives a good background for our studies. Specifically, it gives experimental conditions used by other researchers that may be useful for designing our experiments. IGF-I and IGFBP-3 interaction data is particularly interesting. Data for the experimental conditions is summarized in Table 2.3-1. These experimental conditions give us a starting point for determining experimental conditions used in our experiments. Table 2.3-2 summarizes the rate constants and equilibrium constants from previous studies with SPR using IGF-I and IGFBP-3. These constants will be compared with the constants obtained from our studies at pH 7.4

Table 2.3-1: Summary of Previous Studies with IGF-I and IGFBP-3 – Instrument, Experimental Conditions and Model for Data Fitting

Source	Analyte	Ligand	Instrument	RU Immobilized	Flowrate during Kinetic Experiments	Model for Data Fitting
Heding et al (1996)	**IGF-I**	**IGFBP-3**	BIAcore (unspecified)	650 RU IGFBP-3	8 µl/min	Two-site
Wong et al (1999)	**IGFBP-3**	**IGF-I**	BIAcore X	Not given	8 µl/min	One-site
Dubaquie and Lowman (1999)	**IGFBP-3**	**IGF-I**	BIAcore 2000	400-600 RU	20 µl/min	One-site
Galanis et al (2001)	**IGFBP-3**	**IGF-I**	BIAcore (unspecified)	625 RU	5 µl/min	One-site
Fong et al (2002)	**IGFBP-3**	**IGF-I**	BIAcore X	Not given	5 µl/min	One-site
Fong et al (2002)	**IGF-I**	**IGFBP-3**	BIAcore X	Not given	5 µl/min	One-site
Vorwerk et al (2002)	**IGF-I**	**IGFBP-3**	BIAcore 1000	412 RU	50 µl/min	One-site
Vorwerk et al (2002)	**IGFBP-3**	**IGF-I**	BIAcore 1000	256 RU	50 µl/min	One-site

Table 2.3-2: Summary of Previous Studies with IGF-I and IGFBP-3 – Rate Constants and Equilibrium Affinity Constants

Source	Parameters			
	k_a (M^{-1} s^{-1})	k_d (s^{-1})	K_A (M^{-1})	K_D (M)
Heding et al (1996)	$3.5 \mp 0.37 \times 10^{5}$	$0.78 \mp 0.11 \times 10^{-4}$		$2.3 \mp 0.4 \times 10^{-10}$
Wong et al (1999)	$9.12 \mp 1.65 \times 10^{5}$	$5.32 \mp 0.15 \times 10^{-5}$	$18.4 \mp 3.08 \times 10^{9}$	
Dubaquie and Lowman (1999)	$3.2 \mp 0.5 \times 10^{5}$	$4.7 \mp 0.8 \times 10^{-4}$		$1.5 \mp 0.3 \times 10^{-9}$
Galanis et al (2001)	1.1×10^{-5}	1×10^{-6}	1×10^{11}	
Fong et al (2002)	$0.73 \mp 0.02 \times 10^{5}$	$4.04 \mp 0.75 \times 10^{-4}$	$1.81 \mp 0.34 \times 10^{8}$	
Fong et al (2002)	$21.6 \mp 0.56 \times 10^{5}$	$7.26 \mp 0.19 \times 10^{-4}$	$29.8 \mp 1.09 \times 10^{8}$	
Vorwerk et al (2002)	$7.87 \mp 1.00 \times 10^{5}$	$2.09 \mp 0.35 \times 10^{-4}$	$4.13 \mp 0.71 \times 10^{8}$	

Chapter 3 – Leica Microsystems Bio-SPR 9000

Our overall goal was to use the Leica Microsystems SPR system to determine if a difference in the binding of IGF-I to IGFBP-3 at pH 7.4 and pH 5.8 could be measured using surface plasmon resonance (SPR) and, in particular, determine the association and dissociation constants for the binding of IGF-I to IGFBP-3 at those pHs. This system was chosen because it was a recent gift to Virginia Polytechnic Institute and State University and, therefore, easily accessible.

3.0 Overview of the Chapter

This chapter will discuss the experiments done with the Leica Microsystems SPR instrument. The first part of the chapter will discuss the system setup including a diagram of the system. Following this, the solutions used in these experiments and the experimental procedures used for immobilization of the IGFBP-3 to the surface will be described in detail. A description of the experiments done with this equipment, the results from these experiments and analysis of the data from the experiments are also included in the chapter. A summary of conclusions drawn from these experiments and of further necessary experiments concludes the chapter.

3.1 Leica SPR System Overview

The Leica Bio-SPR 9000 system is composed of several key pieces of equipment: a pump, the solvent selector valve, the SPR biosensor, and a computer (Figure 3.1-1). The pump used for our experiments was a Masterflex® L/S® peristaltic pump (Cole-Parmer Instrument Company, model # 7519-20) fitted with Pharmed® 4 mm O.D., 0.8 mm I.D. tubing. The pump was connected to the valve and biosensor unit with Peek® tubing, 1/16" O.D., 0.02" I.D. The solvent selector valve assembly contains a six-way low pressure selection valve and Peek® tubing for switching between solutions and is in-line between the sensor and the pump. The SPR biosensor is comprised of a BioRefractometer for the measurements and a flow cell for fluid movement in the system. The SPR biosensor is connected to the computer (Hewlett Packard Brio with an Intel® Celeron™ processor, Windows 98 Second Edition) for data acquisition. The computer runs a National Instruments Labview® based software program for handling data and controlling the SPR biosensor.

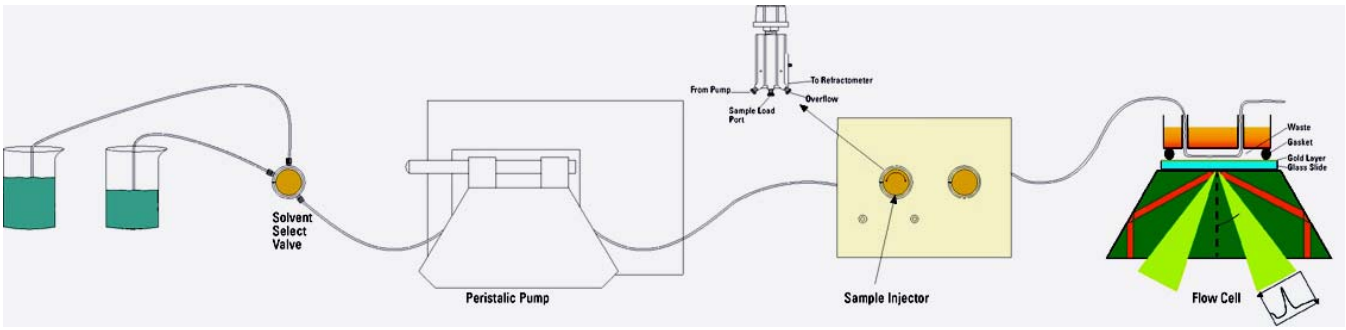

Figure 3.1-1: Diagram of Leica Bio-SPR 9000 System Setup
(Used with permission from Leica Microsystems Inc.)

3.2 Solutions used for SPR Experiments

Two solutions were used for the SPR experiments: a 20 mM sodium acetate buffer and a HEPES-buffered salt solution. To make the sodium acetate buffer, we started with 20 mM acetic acid and titrated to pH 5.5 with 2N sodium hydroxide to yield 20 mM sodium acetate. For the HEPES-buffered salt solution, we placed 700 ml of deionized (DI) water in a 1 L flask and added 7.01 g sodium chloride (120 mM), 0.37 g potassium chloride (5 mM), 0.3 g magnesium sulfate heptahydrate (1.2 mM), 2.0 g sodium acetate trihydrate (15 mM), 1.8 g dextrose (10 mM) and 23.8 g HEPES (100 mM). The solution was then brought up to 1 L total volume with deionized water and filtered through a 0.22 μm cellulose acetate bottle top filter (Corning). Since we were interested in comparing the effect of pH on our reaction, we split the HEPES-buffered salt solution in half and pHed half to 5.8 and half to 7.4 using 1 N sodium hydroxide. All buffers were de-gassed under vacuum before doing any experimental procedures.

3.3 Activation of the Carboxymethylated Dextran Slide and Immobilization of IGFBP-3

We chose to use XanTec CMD 20 (XanTec bioanalytics GmbH, Muenster, Germany) carboxymethylated dextran slides for our studies because the CMD 20 slides are somewhat comparable to the CM 5 chip typically used with the BIAcore System (XanTec 2002). These slides differ in one critical way: the CM 5 chips have a 500,000 molecular weight dextran-coated surface while the XanTec slides use a 20,000 molecular weight dextran. The dextran provides the surface for which our proteins were attached. The attachment process was initiated by placing the slide in the flow cell (Figure 3.3-1). There are several key steps that must be followed to properly place the slide in the unit. First the prism was cleaned using acetone and

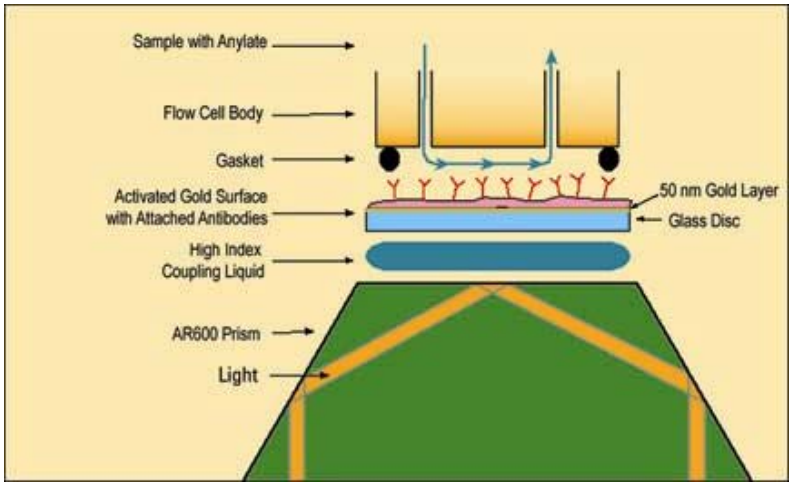

Figure 3.3-1: Exploded View of Flow Cell Showing the Prism, Slide, Gasket and Flow Cell Body
(Used with permission from Leica Microsystems Inc.)

Kimwipes™ until there were no visible streaks on the prism. Dust was blown off of the prism using nitrogen gas. Next two sets of forceps were cleaned with acetone and isopropyl alcohol and dried with nitrogen gas. A 2.5 µl drop of refractive index matching coupling liquid was then placed onto the center of the prism to make sure the glass of the slide is optically coupled to the prism. Then the slide was removed from the package using the clean forceps. The back of the slide was then slowly placed onto the prism and the front gently lowered with the other set of forceps. Once the slide was placed, a gasket was cleaned with isopropyl alcohol and acetone and dried with a Kimwipe™. The gasket was then placed onto the center of the slide using the forceps and centered between the notches on the sides of the flow chamber. The flow cell body was blown dry of dust/particles with nitrogen and the flow cell reassembled by placing the back of the flow cell onto the gasket first and then lowering the front. The cover plate was then placed on the flow cell body and the screws tightened evenly. With the end of the tubing in water, the pump was then turned on and the seal was checked by looking for bubbles coming out of the waste tube.

Once the slide was in place in the unit, deionized water was pumped over the slide to ensure that there were no leaks in the system. We then switched from deionized water to phosphate buffered saline (PBS) pH 7.4 with 0.05% Tween20 detergent (Sigma-Aldrich Corp., St. Louis, MO). The detergent was added to reduce adsorption of the proteins to the plastic tubing.

PBS was run through the system for approximately five minutes until a stable baseline SPR signal was obtained. The EDC/NHS solution (0.076 g N-ethyl-N-(3-diethylaminopropyl) carbodiimide (EDC) and 0.0114 g N-hydroxysuccinimide (NHS) in 2 ml of deionized water) was then injected into the system to activate the surface. This solution ran for approximately ten minutes. Next, the 20 mM sodium acetate buffer (pH 5.5) was run over the sensor surface for approximately five minutes until a stable baseline was obtained. IGFBP-3 solution was injected to allow the protein to bind to the surface. For each run this solution was allowed to flow over the surface for a particular amount of time to obtain the amount of BP-3 desired on the surface. PBS with Tween was run for four minutes to wash the surface. Following the PBS with Tween wash, PBS at pH 8.6 was run for ten minutes to deactivate the surface and prevent covalent binding of other proteins to the slide. To remove BP-3 that did not bind covalently, 10 mM hydrochloric acid with 0.05% Tween was injected for three minutes. To remove the hydrochloric acid from the lines PBS with Tween was run for 5 minutes before switching to the HEPES-buffered salt solution used for the binding experiments. Figure 3.3-2 shows data from a typical IGFBP-3 immobilization.

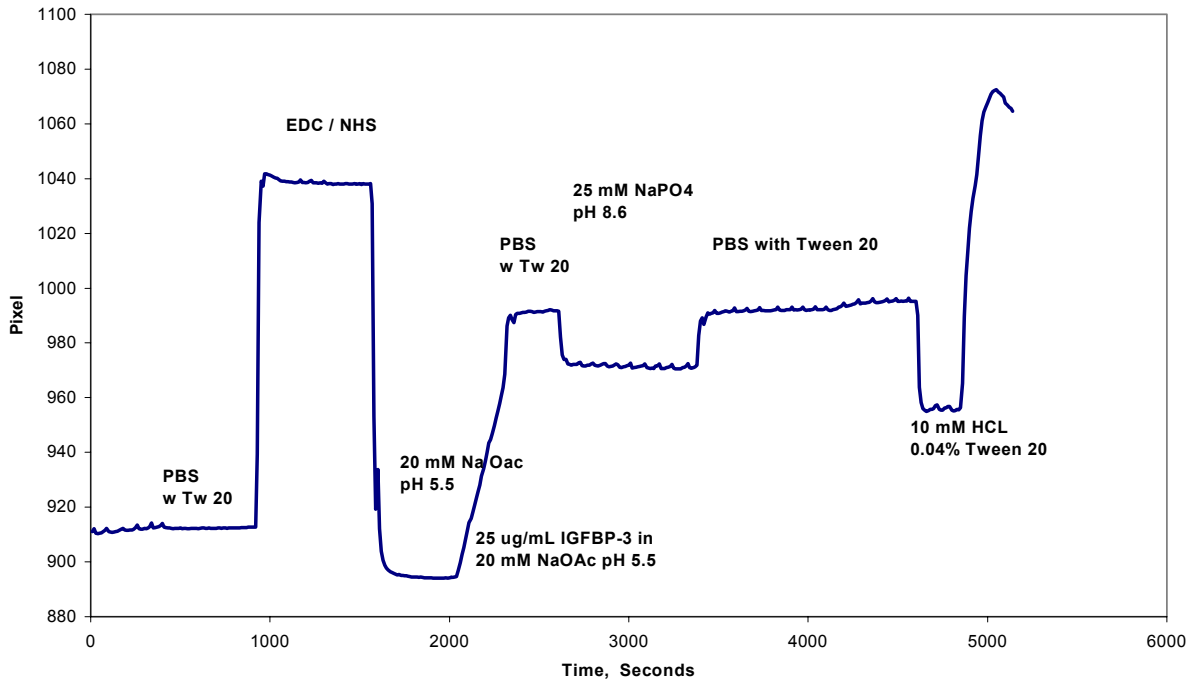

Figure 3.3–2: Immobilization of IGFBP-3 to the CMD20 Slide – Activation of the slide with EDC/NHS is followed by immobilization of IGFBP-3, deactivation of the surface and removal of non-covalently bound proteins with an acid wash

3.4 Preliminary Experiments

3.4.1 Description of Experiment

To test whether or not there was a detectable difference between the binding of the two proteins at the two pH levels, we ran a preliminary test with Thomas Ryan, Business Director of BioAnalytical Solutions, from Leica Microsystems Inc. using a XanTec CMD 20 chip with IGFBP-3 immobilized on it using the procedure described above. The IGFBP-3 solution used in the immobilization process was at a concentration of 50 μg IGFBP-3/ml in 20 mM sodium acetate at pH 5.5. The IGFBP-3 was pumped over the activated surface for 25 minutes to allow for the IGFBP-3 to bind to the surface. Three IGF-I solutions and one insulin solution were run over the sensor surface for the experiment. The solution concentrations were as follows: 0.5 μg IGF-I/ml at pH 7.4, 0.5 μg IGF-I/ml at pH 5.8, 0.25 μg IGF-I/ml at pH 5.8, and 0.5 μg insulin/ml at pH 5.8 in HEPES-buffered salt solution. Insulin was chosen as a negative control since it is approximately the same size as IGF-I but does not bind to IGFBP-3. The tests were initiated by flowing HEPES-buffered salt solution over the sensor surface until a stable baseline was obtained (approximately 10 minutes). Then the sample solution (IGF-I or insulin) was run over the surface for thirteen minutes to allow association. For the dissociation phase, the solution was switched to HEPES-buffered salt solution (without IGF-I or insulin) which was run over the cell for 10 minutes to allow for dissociation. After the dissociation data was collected, the surface was regenerated by flowing 10 mM HCl with Tween over the surface for 3-5 minutes to remove the remaining material bound to the IGFBP-3. This procedure was repeated for each sample.

3.4.2 Results from Preliminary Experiments

The insulin gave no change in refractive index when passed over the immobilized IGFBP-3 indicating that negligible binding had occurred between the insulin and the dextran-bound IGFBP-3 (Figure 3.4.2-1). This was not unexpected as previous studies have indicated that insulin does not bind to IGFBP-3 ((Wong, Fong et al. 1999; Vorwerk, Hohmann et al. 2002)) although at least one Biacore SPR study had suggested slight affinity (Heding, Gill et al. 1996; Vorwerk, Hohmann et al. 2002). Comparison between the signal from the IGF-I, pH 5.8 and IGF-I, pH 7.4 indicated differences both in the slope of the curve and the end peak height (Figure 3.4). The difference in the curves from this preliminary experiment suggested that there

was a difference in the binding at these two pH levels. In order to quantify this difference, a series of kinetic experiments were performed.

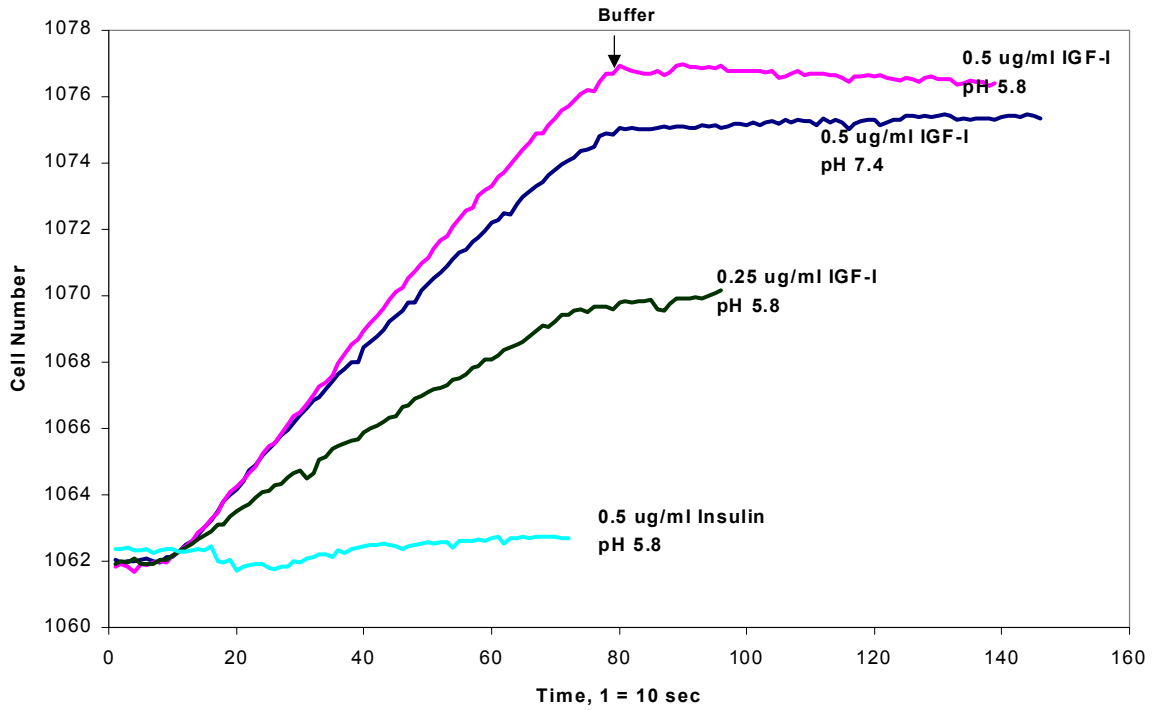

Figure 3.4.2-1: Results from Preliminary Experiment – IGF-I at pH 5.8 shows a higher peak value and different slope than IGF-I at pH 7.4. Insulin shows no binding to immobilized IGFBP-3 as expected

3.5 Initial Kinetic Experiments

3.5.1 Description of Experiments

Previous researchers had investigated IGF-I-IGFBP-3 binding using BIAcore technology at pH 7.4 (Heding, Gill et al. 1996; Dubaquie and Lowman 1999; Wong, Fong et al. 1999; Galanis, Firth et al. 2001; Fong, Wong et al. 2002) and prior to initiating our pH studies, we wanted to validate that the Leica system would provide comparable data. The IGFBP-3 was immobilized on a XanTec CMD 20 chip for this experiment as described above. IGFBP-3 solution (25 µg/ml IGFBP-3 in 20 mM sodium acetate at pH 5.5) pumped through the flow cell to the activated surface for 4 minutes to allow for the IGFBP-3 to bind to the surface. Seven concentrations of IGF-I in the HEPES-buffered salt solutions pH 7.4 were studied: 200 nM, 100 nM, 50 nM, 25 nM, 12 nM, 6 nM, and 3 nM. Each IGF-I solution was allowed to flow over the

immobilized IGFBP-3 for 10 to 14 minutes to allow for association of the proteins. Buffer without IGF-I was then passed over the surface for 5 minutes for collection of dissociation data. The surface was regenerated with HCl between each association/dissociation run as described in the preliminary experiment section.

3.5.2 Results and Data Analysis for Initial Kinetic Experiments

With the Leica system, we were able to detect binding of IGF-I over the entire range of concentrations examined (Figure 3.5). The association curves followed the expected pattern where the higher concentrations led to steeper initial slopes and higher plateau values. The dissociation curves followed the expected pattern of sloping down toward zero.

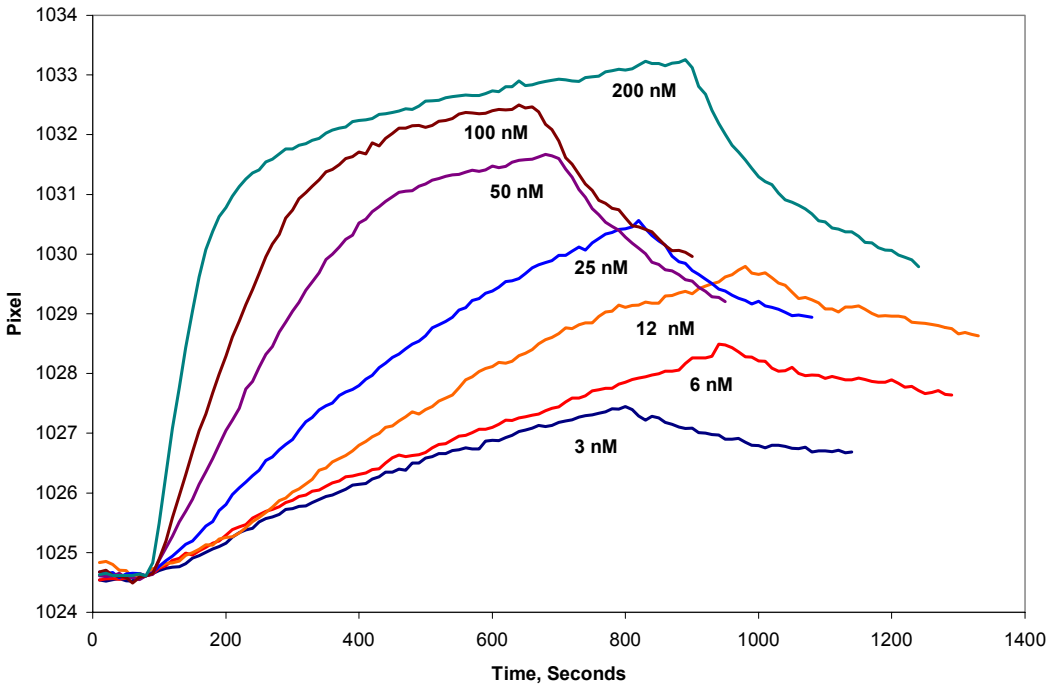

Figure 3.5.2-1: Results from Initial Kinetic Experiments at pH 7.4

The data was analyzed using the one-site model described in Chapter 2. Briefly, each association data set was fit to a single exponential (Eq. 3.1) using Graph Pad Prism

$$R = Y_{\max}\left(1 - e^{-k_{obs}t}\right) \qquad \text{Eq. 3.1}$$

(GraphPad Software, San Diego California USA, www.graphpad.com, Version 3.02 (trial), April 25, 2000). Two parameters were obtained for each concentration, Y_{max} and k_{obs}. Based on the

derivation outlined in Chapter 2, plotting k_{obs} versus the concentration of IGF-I should yield a straight line where the slope is equal to the first-order association rate constant. The first-order dissociation rate constants were obtained by fitting the dissociation data to equation 2.8 b also found in Chapter 2 (Table 3.5.2-1). The values we obtained differed from those of Heding, Gill et al. 1996 (Table 3.5.2-1) suggesting that differences in the experimental conditions using the

Table 3.5.2-1: Comparison of constants from initial kinetic experiments and literature

	k_a (M^{-1} s^{-1})	k_d (s^{-1})	K_D (M^{-1})
Kinetic Experiments	5.00E+04	1.21E-03	2.42E-08
Heding et. al.	3.50E+05	7.80E-05	2.23E-10

two different systems may be at issue. In particular, we were concerned that our set-up may have lead to mass-transport limited binding measurements rather than the desired kinetic parameters. The major contribution to this issue was likely the loading level of the binding protein on the sensor surface.

In our experiment, the immobilization level of binding protein was 79 pixels (approximately 5135 RU) which is significantly higher than the immobilization level of 650 RU (approximately 10 pixels) of Heding et al ((Heding, Gill et al. 1996)). The considerably higher amount of IGFBP-3 on the surface in these experiments may have resulted in crowding effects on the surface. If the binding proteins are very close together, the IGF-I molecules will not be able to bind to the immobilized binding protein without diffusing into the layer of immobilized IGFBP-3. Additionally, the sites may not all be equally accessible due to the large amount of protein on the sensor surface. Initial binding to IGFBP-3 molecules at the top of the dextran differs from binding where the IGF-I has to diffuse into the gel. During the dissociation phase, escape from the gel of IGF-I (via dissociation) will be significantly hindered by rebinding since the IGF-I may be caught in the dextran layer. This likely led to a mass transport step for the diffusion of the IGF-I from the bulk into the IGFBP-3 layer on the surface of the slide and diffusion into the dextran gel. The simple one site model does not account for these types of effects. The possible alternatives were to lower the amount of loading to a level similar to Heding et al. (1996) or to use a more complex model that accounts for the mass transport. We thought using the lower surface loading would help us replicate the results from Heding et al.

(1996) where a simple model was used. The second phase of this work looked at lowering the surface loading to help eliminate the mass transport effects.

3.6 Optimization of Experimental Parameters – Stepwise Immobilization

3.6.1 Description of Experiments

The goal of the next experiments was to immobilize a particular amount of IGFBP-3 on the sensor surface. The surface loading used in most experiments from the literature (Heding, Gill et al. 1996; Dubaquie and Lowman 1999; Galanis, Firth et al. 2001) was less than 1000 RU which translates to 15 pixels. In our previous experiment, 79 pixels (5135 RU) of IGFBP-3 were immobilized. To obtain a lower level of IGFBP-3 on the surface, a stepwise immobilization was used to carefully control the amount of IGFBP-3 on the surface. This was achieved by repeatedly injecting a short (30 second) pulse of the IGFBP-3 solution followed by a wash with PBS. The difference between the PBS level at the beginning of the experiment and after the pulse gave the approximate amount of IGFBP-3 immobilized. The pulses were repeated until approximately 20-23 pixels of IGFBP-3 were immobilized on the surface. After washing and regeneration, our intent was for the surface to have approximately 15-18 pixels of IGFBP-3 immobilized.

3.6.2 Results from Stepwise Immobilization

The stepwise immobilization technique was successful (Figure 3.6.2-1). Using this

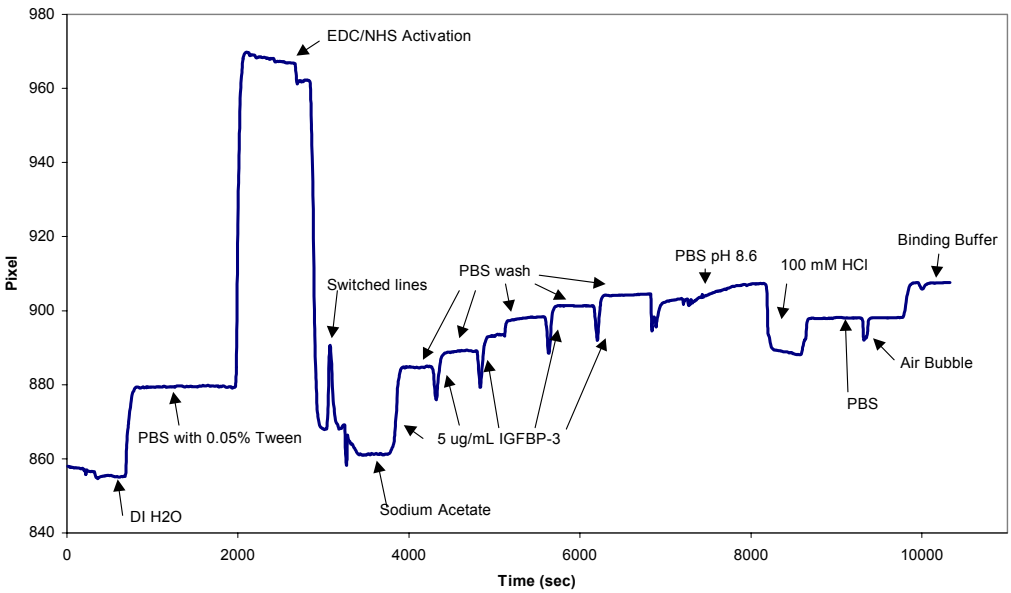

Figure 3.6.2-1: Stepwise Immobilization of IGFBP-3

method a specified level of IGFBP-3 can be immobilized on the surface. However, the reduced amount of BP-3 on the surface lowered the resolution leading to a smaller signal to noise ratio. For example, in Figure 3.7A, high IGFBP-3 loading data leads to a large signal to noise ratio or low noise. In Figure 3.7B, the low loading data has a small signal to noise ratio or high noise. This smaller signal to noise ratio corresponds to noise of the same magnitude as the signal. Alexandr Rafailov, an REU student working in our laboratory, found that the major source of noise in the system was coupling fluid leaking up from under the slide onto the slide surface. Mr. Rafailov spoke with representatives from Leica Microsystems and determined that the oil problem stemmed from new slides that were slightly larger than the slides used previously. This caused the gasket to contact the sides of the flow cell allowing the coupling fluid to wick up onto the surface of the slide. Mr. Rafailov obtained smaller gaskets that did not touch the sides of the flow chamber from Leica Microsystems and reduced the amount of coupling fluid used from 2.5 µl to 0.2 µl. These modifications raised the signal to noise ratio to an acceptable level and kinetics experiments were run.

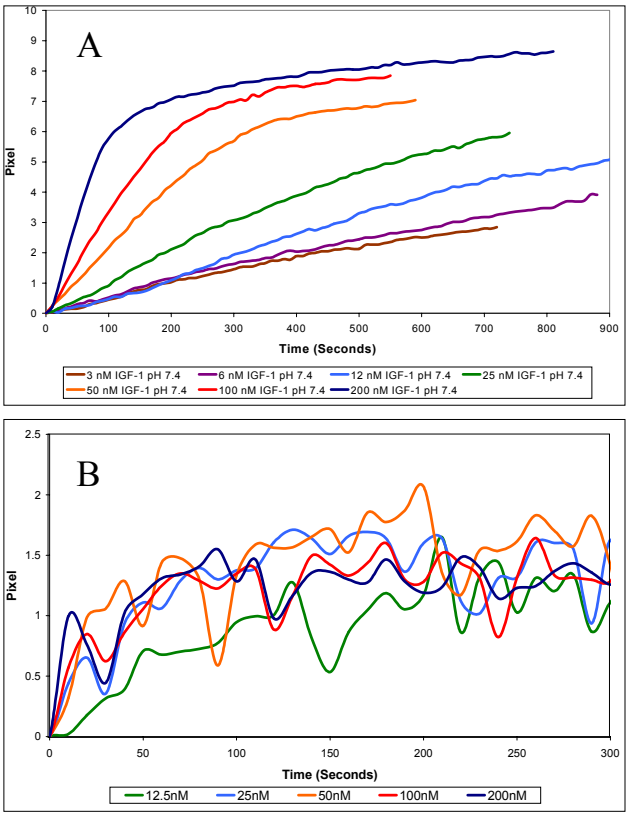

Figure 3.6.2-2: Noise Comparison **A**: Data from High loading experiment – low noise **B**: Data from Low loading experiment – high noise

3.7 Modified Kinetics Experiments

3.7.1 Description of Experiments

Three complete kinetics experiments at both pH 7.4 and 5.8 were run on CMD 20 slides using the lower loading protocol. The IGFBP-3 was immobilized in the stepwise manner described above. For each experiment, five concentrations of IGF-I at pH 7.4 were exposed to the sensor surface: 200 nM, 100 nM, 50 nM, 25 nM, and 12.5 nM. Two replicates were taken for each concentration. The entire experiment was repeated on the same sensor surface for pH 5.8.

3.7.2 Results and Data Analysis for Modified Kinetics Experiments

In this experiment we were able to detect binding of IGF-I over the entire range of concentrations examined (Figure 3.7.2-1). The association curves followed the expected pattern where the higher concentrations led to steeper slopes and higher plateau values. The dissociation curves follow the expected pattern by sloping down toward zero. Data was fit to the one site

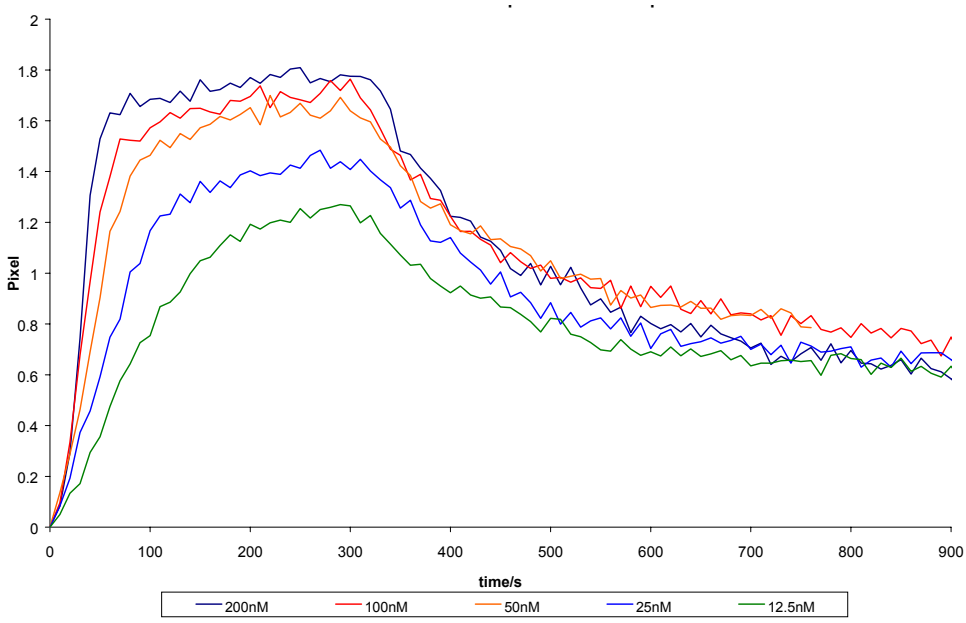

Figure 3.7.2-1: Representative Data from Modified Kinetic Experiments – pH 5.8. The association phase runs from time equals zero to time equals 320 seconds and the dissociation phase starts at time equals 320 seconds

model described previously. Following the data analysis, the association and dissociation constants for the two pHs were not significantly different due to the large variation in the constants obtained from each experiment (Table 3.7.2-1). While this was surprising, the real

issue arose from our analysis of the fit. The residuals (Figure 3.7.2-2) from these fits showed a definite pattern indicating model mismatch and that there may still be mass transport effects in

Table 3.7.2-1: Kinetic Parameters from Modified Kinetic Experiments ± Std. Dev.

pH 7.4			pH 5.8		
$k_{on}/10^{-4}nM^{-1}s^{-1}$	$k_{off}/10^{-3}s^{-1}$	K_D/nM	$k_{on}/10^{-4}nM^{-1}s^{-1}$	$k_{off}/10^{-3}s^{-1}$	K_D/nM
1.24 ±0.42	6.94 ±2.90	56.1 ±30.2	1.20 ±0.26	5.36 ±4.03	44.7 ±35.0

our system. Unfortunately, using a lower surface loading to reduce these effects would likely make the signal to noise ratio too low to distinguish the SPR signal from the noise. Using an instrument with a higher signal to noise ratio might allow us to determine these constants more accurately.

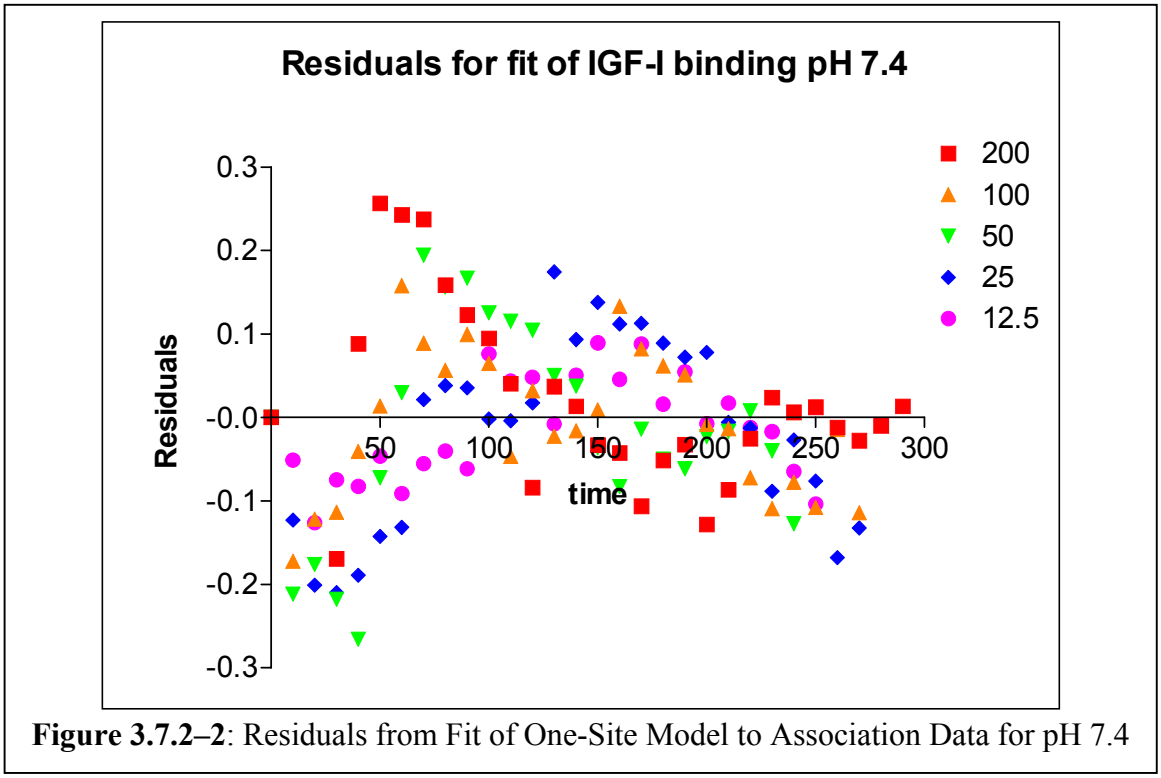

Figure 3.7.2–2: Residuals from Fit of One-Site Model to Association Data for pH 7.4

3.8 Conclusions and Further Experimentation

The association and dissociation constants could not be determined accurately with this instrument due to the large variability between the results from the three experiments. Due to this variability, we decided to investigate using a BIAcore 2000 instrument available to us at

MIT through Professor Douglas A. Lauffenburger to measure the desired parameters. We hypothesized that the increased control over the flow rate and higher signal to noise ratio of the BIAcore 2000 instrument might allow us to make the desired measurements and would allow us to duplicate the experimental conditions found in Heding et al. (1996). The results from studies on the BIAcore 2000 instrument at MIT are described in Chapter 4.

Chapter 4 – BIAcore 2000

Our results from studies using the BIAcore® 2000 instrument at MIT are described in this chapter. Our goal was to use the BIAcore® 2000 SPR system to measure the association and dissociation constants for the binding of IGF-I to IGFBP-3 at pH 7.4 and 5.8. Due to the issues found with the Leica Microsystems SPR system (Chapter 3), we decided to investigate the binding using a BIAcore® 2000 instrument available to us at MIT through Professor Douglas A. Lauffenburger. We postulated that the increased control over the flow rate and higher signal to noise ratio of the BIAcore® 2000 instrument might allow us to make the desired measurements and would also allow us to duplicate the experimental conditions found in a previous study investigating IGF-I-IGFBP-3 binding at physiologic pH (Heding et al. 1996).

4.0 Overview of the Chapter

This chapter will describe in detail the experiments done with the BIAcore® 2000 instrument at MIT. The first part of the chapter will discuss the system setup. Following this, the solutions used in these experiments and the experimental procedures used will be described in detail. The results from the experiments and analysis of the data from the experiments are also included in this chapter. A summary of conclusions drawn from these experiments and of further necessary experiments concludes the chapter.

4.1 BIAcore® 2000 System Setup

The BIAcore® 2000 instrument (Biacore International AB, Uppsala, Sweden) consists of a liquid handling system with precision pumps, an integrated fluidic cartridge (IFC), temperature control, an optical system and a separate personal computer for data acquisition (Biacore AB 2002). The liquid handling system contains an autosampler that can transfer, mix, dilute and inject samples into the detection flow cell (Biacore AB 1996). It also contains two stepper motor-driven syringe pumps, one for autosampler functions and one for continuous flow (Biacore AB 1996). The system can obtain flow rates through the flow cell in the range of 1 – 100 μl/min (Biacore AB 1996). The IFC consists of four flow channels in a polymer plate, sample loops, and pneumatically actuated diaphragm valves. The IFC controls delivery of the sample to the sensor chip surface and is pressed into contact with the sensor surface (Pharmacia Biosensor AB 1994). The microfluidics allow for rapid exchange of sample and buffer at the

sensor surface and provide the ability to precisely control the contact time of the sample with the sensor chip (Pharmacia Biosensor AB 1994). The temperature control unit maintains the temperature at the sensor surface and can be set between 4 and 40 °C (Biacore AB 1996). The optical system uses a fixed array of diode detectors to monitor the position of the resonance angle that is expressed in resonance units. A microcomputer in the instrument collects data from the diode detector arrays and controls the instrument (Pharmacia Biosensor AB 1994). The personal computer that interfaces with the system uses Windows 95® operating system and runs the Biacore® Control 2.0 software (Biacore International AB, Uppsala, Sweden). The Biacore® Control software is used to design experiments, control the automated BIAcore system during experiments and save data for analysis (Pharmacia Biosensor AB 1994). The data is displayed as the experiment is run in a sensorgram that is the SPR signal in resonance units (RU) versus time in seconds.

4.2 Materials Used for SPR Experiments

Two solutions were used for the SPR experiments: a 20 mM sodium acetate buffer and a HEPES-buffered salt solution. Each solution was also used with the Leica system and are described in Chapter 3. For these experiments 0.005% Tween 20 detergent was added to the HEPES-buffered salt solution to minimize adsorption of proteins to the tubing in the SPR system. All buffers were de-gassed under vacuum before doing any experiments.

Other supplies used for these experiments are a BIAcore Amine Coupling Kit (BIAcore International AB, Uppsala, Sweden), BIAcore 7 mm plastic vials with caps, and 100 mM HCL for regeneration. The Amine Coupling Kit consists of 750 mg of N-Ethyl-N'- (3-dimethylaminopropyl)-carbodiimide hydrochloride (EDC), 115 mg of N-Hydroxysuccinimide (NHS) and 10.5 ml of 1 M ethanolamine hydrochloride-NaOH pH 8.5. To prepare the reagents for the experiments, 10 ml DI H_2O was added to the EDC vial and 10 ml of DI H2O was added to the NHS vial. These vials were capped and agitated until all solids were completely dissolved. The EDC, NHS and ethanolamine were then aliquoted into 7 mm plastic vials, capped and frozen at –20 °C until needed. The 100 mM HCL was made by diluting 1 M HCL (Fisher Scientific, Pittsburgh, PA) to the concentration needed with DI H2O.

We used research grade CM 5 chips from BIAcore (Biacore International AB, Uppsala, Sweden). These surfaces differ from the XanTec slides used with the Leica System (Chapter 3) in that the BIAcore CM 5 chips have a 500,000 molecular weight dextran and the XanTec slides use a 20,000 molecular weight dextran. These chips were used because they are the recommended sensor chip for this type of protein–protein interaction (Roush, Personal Communication).

4.3 Activation of the Carboxymethylated Dextran Chip and Immobilization of IGFBP-3

The first step in the process was to load a sensor chip into the docking port. The dock command in Biacore Control was then used to correctly position the chip for the experiment. The next step is to use the Prime command which flows buffer over the sensor chip for seven minutes to fill the tubing with buffer and primes the pumps. For this part of the experiment the flow rate was set to 5 μl/min. The next step was to change the settings to allow solution to run over only flow cell four. Using the dilute command, we mixed 1 part NHS solution with 1 part EDC solution and then injected 35 μl of EDC/NHS solution over the sensor surface to activate the chip using the "Quickinject" command. Using the Inject command, 10 μl of a 10 μg/ml solution of IGFBP-3 was injected over the sensor surface to immobilize the protein. This resulted in 1600 – 1700 RU of IGFBP-3 immobilized on chip 2 and 930 RU immobilized on chip 1. The Quickinject command was used next to inject 35 μl of 1 M ethanolamine hydrochloride-NaOH (pH 8.5) which deactivates the carboxymethylated dextran on the surface. To remove solutions from the lines all four flow cells were flushed with buffer for two minutes at a flow rate of 10 μl/min. This procedure was repeated for flow cells two and three. Flow cell one was left blank as a reference cell. After immobilization was completed for all flow cells, 50 μl of 100 mM hydrochloric acid was injected over all four sensor surfaces to regenerate the surface.

4.4 Procedure for Kinetics Experiments on BIAcore® 2000

To perform kinetic experiments on the BIAcore® 2000, a program was written to input the commands to the computer (Figure 4.4-2). This program was based on the sample kinetic program in the Biacore Control software (Biacore International AB, Uppsala, Sweden). The first section of the program defined a function named *kinetic* to run an injection of one concentration of IGF-I. The first three lines set up commands for the rest of the program. The PARAM

statement gave the parameters that accompany the command: the position of the IGF-I solution in the sample holder rack, *analytepos*, the concentration of the IGF-I solution, *conc*, and the pH of the solution, *ph*. The KEYWORD statement denotes the units for the concentration value, *nM*. The CAPTION statement provided a title for the sensorgram. The flow rate was set to 10 µl/min by using the FLOW command. FLOWPATH 1,2,3,4 set the solutions to be run over all four flow cells in series (Figure 4.4-1). The KINJECT command told the instrument to inject 50 µl of the solution in the position given over the sensor surface and to allow for 600 seconds of dissociation time. A data point was taken ten seconds before the start of the KINJECT command to give a baseline for the amount of ligand on the surface by using the RPOINT command. The INJECT command was used to inject 20 µl of the regeneration solution, 100 mM HCl, over the sensor surface to remove the IGF-I. EXTRACLEAN was used to wash the flow cell area and

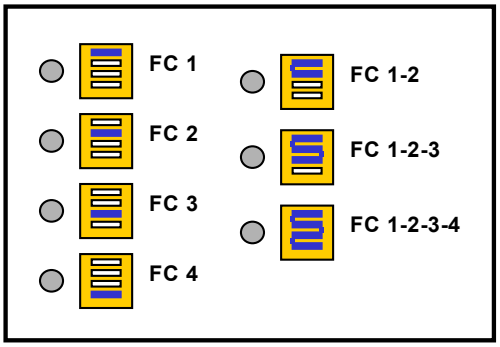

Figure 4.4-1: Flow Cell Setups for BIAcore 2000
(Redrawn from http://www.biacore.com)

tubing after regeneration. Report points were taken to note the RU level for the analyte and a baseline after the washing procedures are complete. The second section of the program was the main code used for the procedure (Figure 4.4-2). The first two statements told the instrument which racks were in the machine. The third statement told the computer to take data in all four flow cells. The kinetic program defined in the first part of the program was then run five times, once for each concentration of IGF-I tested: 200 nM, 100 nM, 50 nM, 25 nM and 12.5 nM. After that, the APPEND CONTINUE line told the instrument to run buffer continuously after the procedure was completed. Each data set was normalized in BIAevaluation™ 3.1 software (Biacore International AB, Uppsala, Sweden) and exported as a text file for analysis in Graph Pad Prism (GraphPad Software, San Diego California USA, www.graphpad.com, Version 3.02 (trial), April 25, 2000).

```
BIAcore method for kinetic analysis - five concentrations of analyte

DEFINE APROG kinetic
     PARAM %analytepos %conc %ph
     KEYWORD nM %conc
     CAPTION %conc nM IGF-1 pH %ph

     FLOW      10
     FLOWPATH  1,2,3,4
   * KINJECT   %analytepos 50 600    !pos, vol and dissociation time
 -0:10 RPOINT    -b ligand
   * INJECT    R2F3 20               !regeneration of the ligand-analyte complex
     EXTRACLEAN                     !Extra washing procedure of the flow cell area
                                    !recommended after regeneration pulses
 -0:10 RPOINT    -b analyte
  5:20 RPOINT    BASELINE2
END


MAIN
     RACK      1 thermo_c
     RACK      2 thermo_a
     FLOWCELL  1,2,3,4              !Sensorgram in flow cell 1,2,3,4

     APROG     kinetic R2C1 200   7.4
     APROG     kinetic R2C2 50    7.4
     APROG     kinetic R2C3 12.5  7.4
     APROG     kinetic R2C4 100   7.4
     APROG     kinetic R2C5 25    7.4

     APPEND    CONTINUE            !Continuous flow after aprog
END
```

Figure 4.4-2: Biacore Control Program for Kinetic Experiments – This program inputs commands into the computer for kinetic experiments on the BIAcore 2000.

4.5 Results

Data from one flow cell (FC4) on chip 1 is shown in Figure 4.5-1. This flow cell had 930 RU of IGFBP-3 immobilized on the CMD surface. The response is as expected for the association phase. The concentrations are in order increasing in slope from the lowest concentration to the highest concentration. In general, higher concentrations reach higher peak

values although the 50 nM sensorgram overlapped the 100 nM sensorgram. In the dissociation phase the sensorgrams do not tend to slope down toward zero as expected. Some concentrations have an upward slope and some concentrations tend to slope slightly downward but none appear to approach zero.

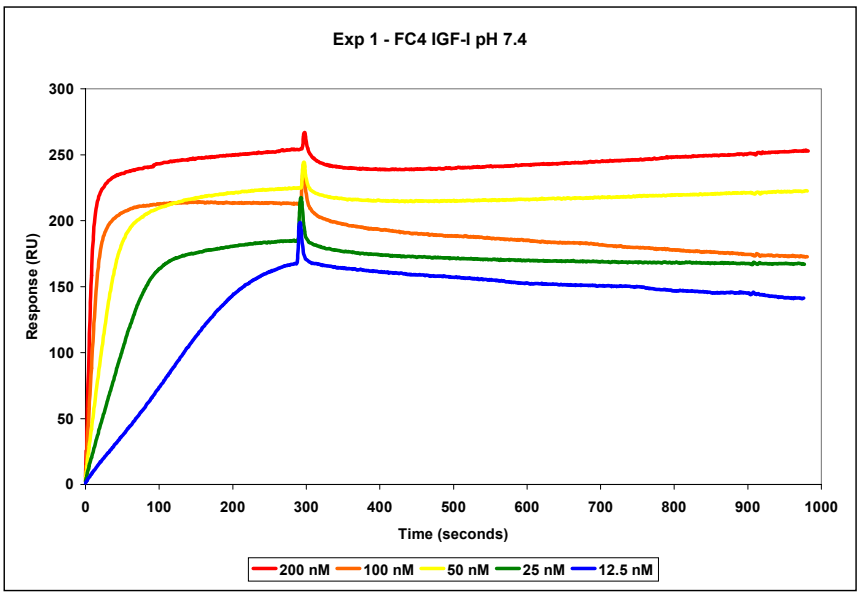

Figure 4.5-1: Data from Experiment at pH 7.4 on Flow Cell 4 of Chip 1

On chip 2 flow cells 3 and 4 contained data for IGFBP-3 immobilized (Figure 4.5-2). Flow cell four had 1727 RU of IGFBP-3 immobilized and flow cell 3 had 1612 RU of IGFBP-3

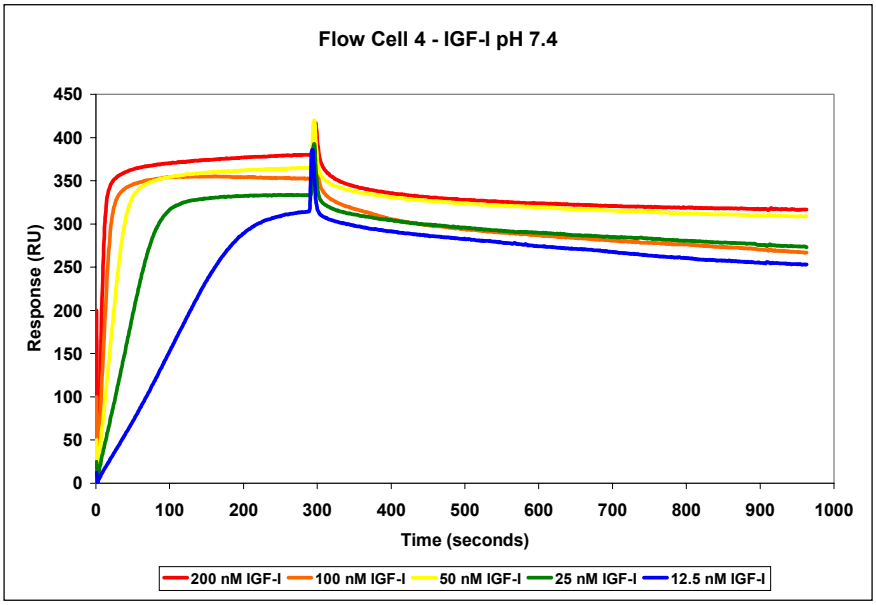

Figure 4.5-2: Data from Experiment at pH 7.4 on Flow Cell 4 of Chip 2

immobilized. The response is as expected for association and is similar to the results seen on chip 1 with the concentrations in order and the highest concentration reaching the highest peak value. Again the sensorgram for 50 nM IGF-I overlaps the sensorgram for 100 nM. On this chip, the dissociation curves all have a downward trend but do not appear to approach zero.

4.6 Data Analysis

We first analyzed the data using the one site model (described in Chapter 2). For both immobilization levels the fit lines do not go through the data and the residuals show a pattern indicating model mismatch (Ott and Longnecker 2001). Association data is shown in figures 4.6-1 A and 4.6-1 B. The dissociation phase data shows model mismatch as well.

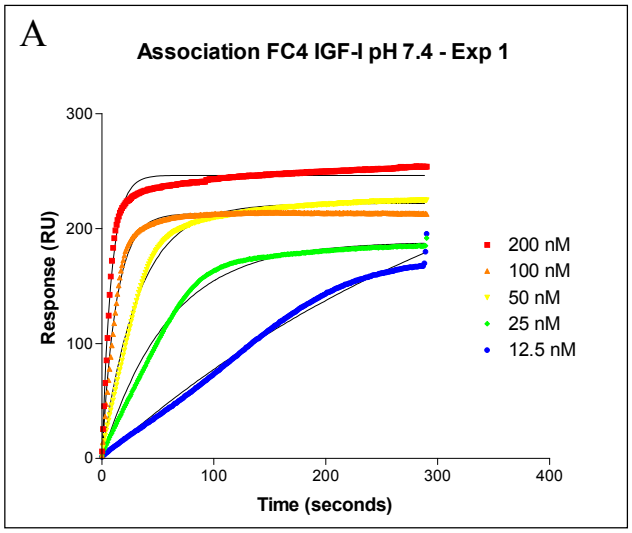

Figure 4.6-1: Fit of Association Data with One-Site Model **A:** 930 RU immobilization – Association Data for pH 7.4 Black lines are fit of the data with the one-site model **B:** Residuals from fit of one-site model

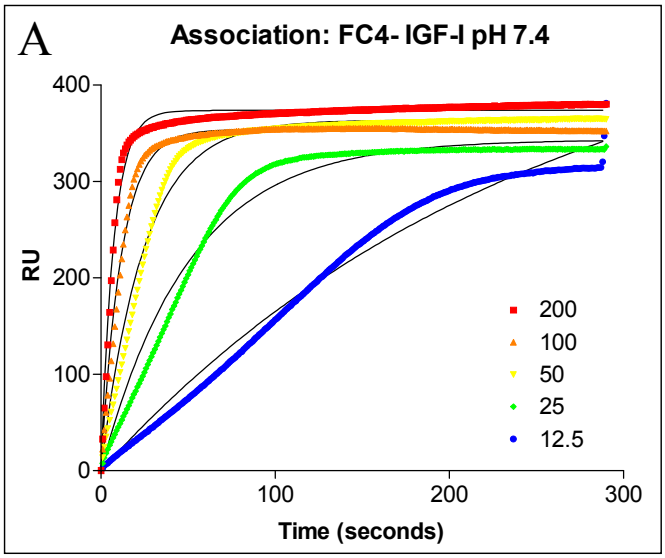

Figure 4.6-2: Fit of Association Data with One-Site Model **A**: 1600 RU immobilization- Association Data for pH 7.4 Black lines show fit of data with one-site model **B**: Residuals from fit of one-site model

The interaction between IGF-I and IGFBP-3 is believed to be first-order (Dubaquie and Lowman 1999; Wong, Fong et al. 1999; Galanis, Firth et al. 2001; Fong, Wong et al. 2002), there may be an additional (low affinity) site due to immobilization. For example, Heding, Gill et al. 1996 state that their data was fit well by a two-site model described in Chapter 2. We fit the data to this two-site model using Graph Pad Prism software (GraphPad Software, San Diego California USA, www.graphpad.com, Version 3.02 (trial), April 25, 2000). For this model, the fit lines clearly do not match well with the data and the residuals show a pattern reflecting model

mismatch (Ott and Longnecker 2001). We reviewed current literature for possible causes relating to model mismatch in SPR.

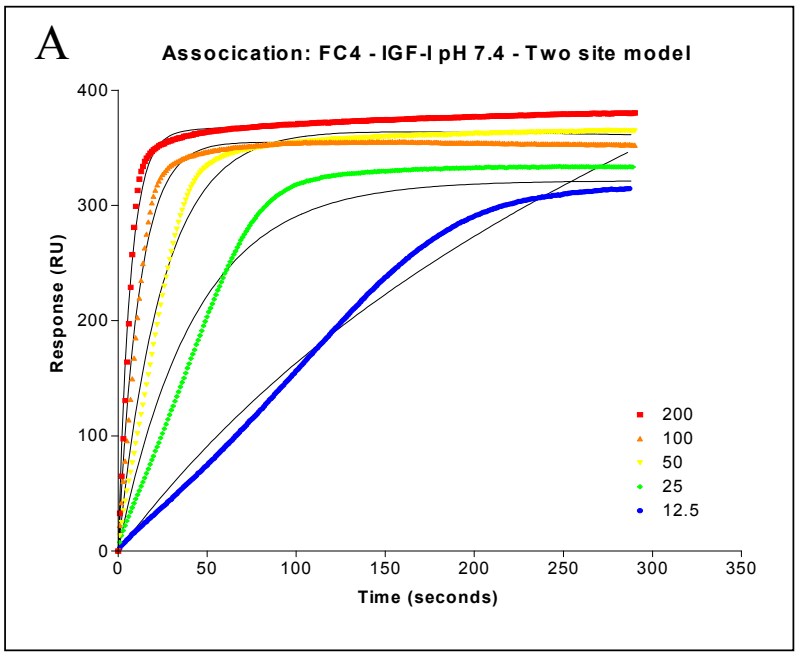

Figure 4.6-3: Fit of Association Data with Two-Site Model **A:** Fit of Association data for 1600 RU immobilization to two-site model **B:** Residuals from fit of two site model

One possible explanation for the poor fit of the one-site model to the data is that the model assumes rapid mixing throughout the flow cell. This model does not account for mass transport from the bulk phase to the sensor surface. A 1996 paper by Schuck and Minton suggests tests for mass transport limitations. Shuck and Minton indicate that plotting dR/dt vs. R for the association phase and plotting ln(Ro/R) vs. t-to in the dissociation phase can help to test for mass transport limitations in the data. The plots should be straight lines if the data can be fit to the one-site model. If there is curvature in the data there may be mass transport limitations.

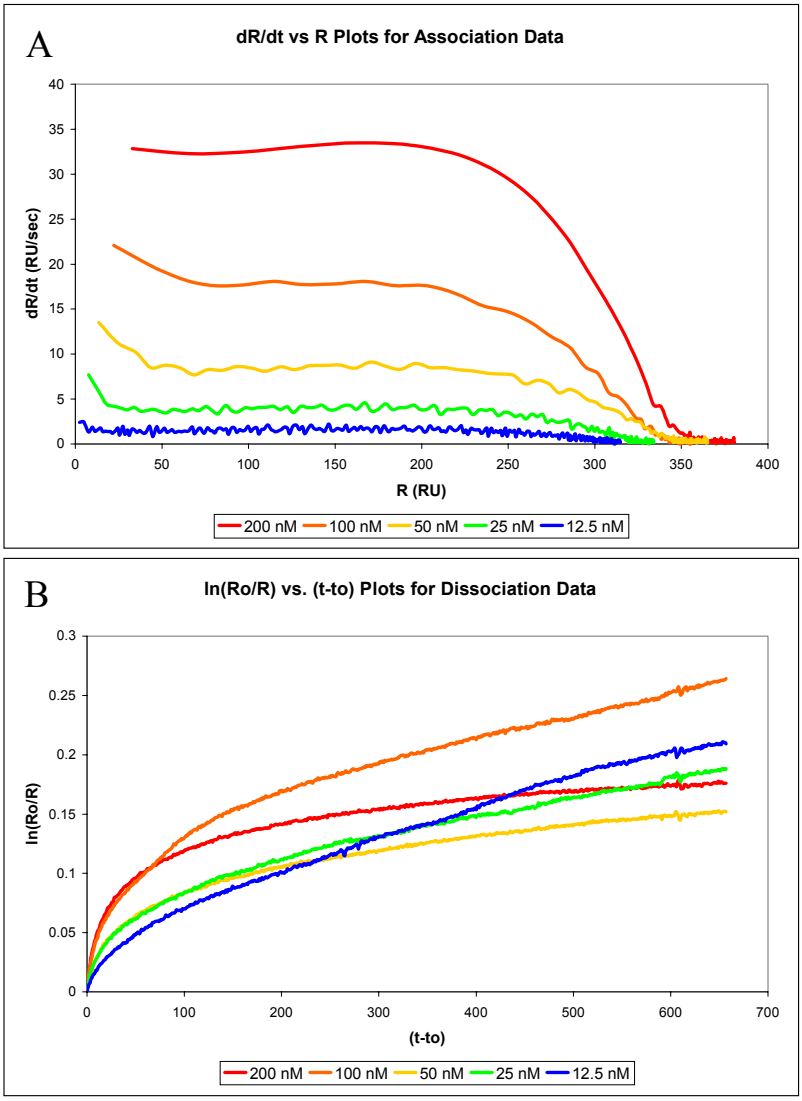

Figure 4.6-4: Test for Mass Transport Limitations **A**: dR/dt plot for association data - Curvature in plots indicates possible mass transport limitations **B**: ln Ro/R plot for dissociation data – Curvature in plots indicates possible mass transport

Our data showed curvature when plotted (Figure 4.6-4), indicative of mass transport limitations (Schuck and Minton 1996). Based on work by David Myszka et al suggesting a two-compartment model to account for transport from the bulk to the sensor surface, we extended our analysis to include this more complex model. In the two-compartment model, the first compartment accounts for transport of the analyte from the bulk solution to the surface with binding of the analyte to the ligand occurring the second compartment (see Chapter 2 Eq. 2.18, 2.19 and 2.20). CLAMP, freely available software written by Morton and Myszka (Morton and Myszka 1998; Myszka, He et al. 1998), uses a global analysis to fit the association and dissociation phase data at the same time based on this model and we used it for the analysis (Figure 4.6-5).

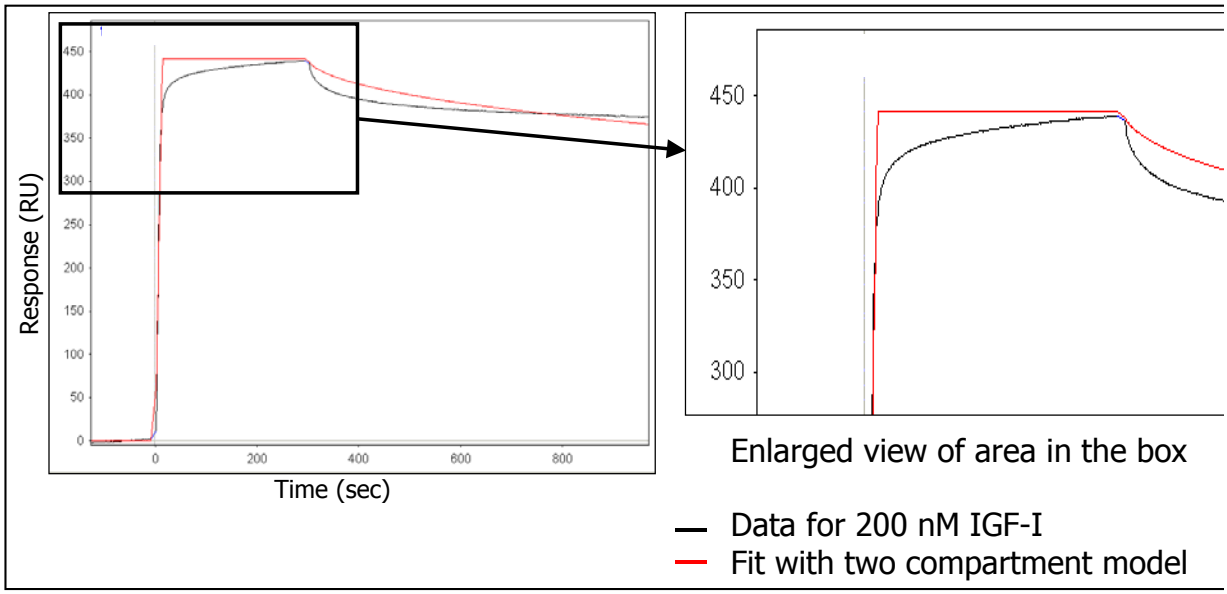

Figure 4.6-5: Fit of data with Two-Compartment Mass Transport Model using CLAMP

The fit however was not appropriate as evident by the mismatch of the red (fit) and black (data) lines (Figure 4.6-5). Two possible explanations for this mismatch are that (1) a more complex binding interaction between IGF-I and IGFBP-3 or (2) mass transport in the dextran layer. The mass-transport model includes only transport from the bulk phase to the sensor surface. This model assumes that the dextran layer has no effect on the association or dissociation rates. However, the dextran layer may present a barrier to diffusion. This would cause a mass transport term for diffusion into the dextran to be present in the system (Schuck 1996). Because of this diffusion limitation, there may also be inhomogenaety in the

immobilization of IGFBP-3 creating a concentration gradient within the dextran layer (Schuck 1996). Since the dextran layer is relatively thick (100-200 nM (Earp 1998)) inhomogenaety in the distribution of IGFBP-3 molecules throughout the dextran layer leading to mass transport of the IGF-I into the dextran layer is the most likely cause of the model mismatch.

Two possible solutions to the mismatch problem are to develop a complex model to explain the interaction between the two proteins, or, to alter the experimental protocol and take data under conditions where the assumptions of the one-site model are met. Developing a more complex model is difficult since the exact conditions on the sensor surface are unknown. For example, in order to come up with a more accurate model, the concentration and distribution of the immobilized IGFBP-3 would need to be precisely determined. Currently, this is not something that can be done with the BIAcore instrument and would be difficult to measure without new experimental tools. Altering the experimental protocol so the model assumptions are valid is the most viable option. The major assumptions of the one-site model are rapid mixing throughout the flow cell (no mass transfer from bulk to surface or into dextran layer) and one IGF-I molecule binds to one IGFBP-3 molecule. Given the biological evidence for a one-to-one interaction between IGF-I and IGFBP-3 (Dubaquie and Lowman 1999; Wong, Fong et al. 1999; Galanis Firth et al. 2001; Fong, Wong et al. 2002), we will concentrate on how to meet the rapid mixing assumption. Rapid mixing can be achieved by increasing the flow rate of solution through the flow cell and using lower concentrations of ligand on the surface to avoid steric hindrance from molecules being located in close proximity to one another. Another way to achieve rapid mixing and avoid mass transport is to use a sensor surface without a carboxymethylated dextran layer.

Increasing the flow rate and using lower surface loading should eliminate mass transport effects from the bulk solution to the surface. The lower analyte concentrations from our previous experiments seem to have the least mass transport effects suggesting that these lower concentrations are more appropriate levels for our experiments. We also propose using a different surface to avoid mass transport within the dextran layer. A planar surface with no dextran gel would avoid the transport issues found with the thick dextran used in the BIAcore CM5 chip.

Working with Tom Ryan of Leica Microsystems Inc., a planar carboxylated surface made by XanTec (XanTec bioanalytics, Muenster, Germany) and a planar carboxylated mSAM surface made at Cornell via a procedure from Lahiri, Isaacs et al. (1999) became available for use. In addition, Leica Microsystems Inc. developed a new instrument, SPR 2001 Alpha, in 2002 with improved signal to noise ratio and a smaller flow cell requiring less protein solution. The improvements in this device will allow for lower surface loading without the noise problems that plagued our earlier experiments (Chapter 3).

4.7 Conclusions

A BIAcore® 2000 instrument available to us at MIT through Dr. Douglas A. Lauffenburger was used for the studies described in this chapter. The data obtained from the studies was fit to the one-site, the two-site and the mass transport limited model. The fits of the data to all these models show evidence of model mismatch. We determined that a more complicated model would be needed to obtain kinetic rate constants from this data. Since a more complex model would be difficult to develop without detailed knowledge of what was occurring on the sensor surface we decided that an altered experimental protocol should be used to help elucidate the kinetic rate constants. Specifically we think using higher flow rates, lower surface loading of ligand, and lower analyte concentrations will help avoid the mass transport issues seen in these experiments. In addition the thick carboxymethyl dextran layer used in these experiments may cause additional mass transport issues. Using a self-assembled monolayer planar surface should eliminate mass transport by the dextran gel. Leica Microsystems Inc. has new SPR equipment and new surfaces that meet our altered experimental conditions. We decided to try experiments with altered experimental protocol on Leica Microsystems new SPR 2001 Alpha with the planar surfaces. The results from this effort are discussed in Chapter 5.

Chapter 5 – Leica Microsystems SPR 2001 Alpha

Our results from studies using the Leica Microsystems SPR 2001 Alpha are described in this chapter. Our goal was to use the SPR 2001 Alpha system with a planar surface to measure the association and dissociation constants for the binding of IGF-I to IGFBP-3 at pH 7.4 and 5.8. Due to the mass transport effects and model mismatch in the data from the BIAcore® 2000 (Chapter 4), we decided to investigate the binding using a Leica Microsystems Inc. SPR 2001 Alpha instrument available to us through Thomas Ryan at Leica Microsystems Inc., Analytical and Educational Services Division in Buffalo, NY. We felt that the ability to use a planar surface and the improved signal to noise ratio of the SPR 2001 Alpha instrument might allow us to make the desired measurements.

5.0 Overview of the Chapter

This chapter will discuss the experiments done with the Leica Microsystems SPR 2001 Alpha instrument using the new planar surface chips. These studies were performed at Leica Microsystems Inc. Analytical and Educational Services Division in Buffalo, NY with the assistance of Thomas E. Ryan and Thor H. Roalsvig. The first part of the chapter deals with the system setup. Following this, the solutions used in these experiments and the experimental procedures used for immobilization of the IGF-I to the surface are described in detail. A description of the experiments done with this equipment, the results from these experiments and analysis of the data from the experiments are also included in the chapter. A summary of conclusions drawn from these experiments and of further necessary experiments concludes the chapter.

5.1 Leica SPR System Overview

The Leica SPR 2001 Alpha system is composed of several key pieces of equipment: a pump, the solvent selector valve, the SPR biosensor and a computer. One of two pumps was used for each of our experiments, a peristaltic pump or a syringe pump. The peristaltic pump used for our experiments was a WIZ® peristaltic pump (Isco, Inc., Lincoln, Nebraska model # 1610-004) fitted with Pharmed® 4 mm O.D., 0.8 mm I.D. tubing. The syringe pump used was a Hamilton syringe pump (Hamilton Company, Reno, NV) fitted with two 25 ml syringes from Hamilton Company and Pharmed® 4 mm O.D., 0.8 mm I.D. tubing. The pump was connected to

the valve and biosensor unit with Peek® tubing, 1/16" O.D., 0.02" I.D. The solvent selector valve assembly contains a six-way low pressure selection valve and Peek® tubing for switching between solutions and an injection port and is in line between the sensor and the pump. The SPR biosensor is comprised of a BioRefractometer for the measurements, a Peltier device for temperature control and a flow cell for fluid movement in the system. The SPR biosensor is connected to the computer (Hewlett Packard Brio with an Intel® Celeron™ processor, Windows 98 Second Edition) for data acquisition. The computer runs a National Instruments Labview® based software program for handling data and controlling the SPR biosensor (Figure 5.1-1).

Figure 5.1-1: Leica Microsystems SPR 2001 Alpha System with peristaltic pump (Used with permission of Leica Microsystems Inc.)

This system differs from the Leica system used for the studies in Chapter 3, the Leica Bio-SPR 9000, in three major ways. The first is that the new system uses a considerably smaller flow cell. The flow cell used in chapter three had a length of 10.8 mm, a width of 4 mm and a height of 0.19 mm. The height of the flow cell is given using the assumption that the gasket is 50% compressed (Ryan, Personal Communication). The volume of this flow cell using an oval gasket was 9.94 μl (Ryan, Personal Communication). The flow cell used in the new system had a length of 8.5 mm, a width of 1.5 mm and a height of 0.19 mm (Ryan, Personal

Communication). The volume of this flow cell using an oval gasket was 2.33 µl (Ryan, Personal Communication). The second difference is that the SPR 2001 Alpha has significantly less noise than the previous Leica system. The SPR 2001 Alpha has a peak to peak noise of around 0.05 pixel (Ryan, Personal Communication) while the noise on the older Leica Bio-SPR 9000 was around 0.1 pixels. The third difference is that the system used in chapter three did not have a temperature control device while the SPR 2001 Alpha uses a Peltier temperature control device to maintain the temperature at a constant set point throughout the experiment. The use of this device provided us with constant temperature for more than eight hours while running an experiment. This was important because the refractive index of a solution is dependent on temperature. Figure 5.1 shows a graph of the response on one y-axis, the temperature on the other y-axis and time on the x-axis for one of the experiments described later in this chapter. This graph shows that temperature fluctuates slightly throughout the course of the experiment and that the response is not affected by these slight changes in temperature.

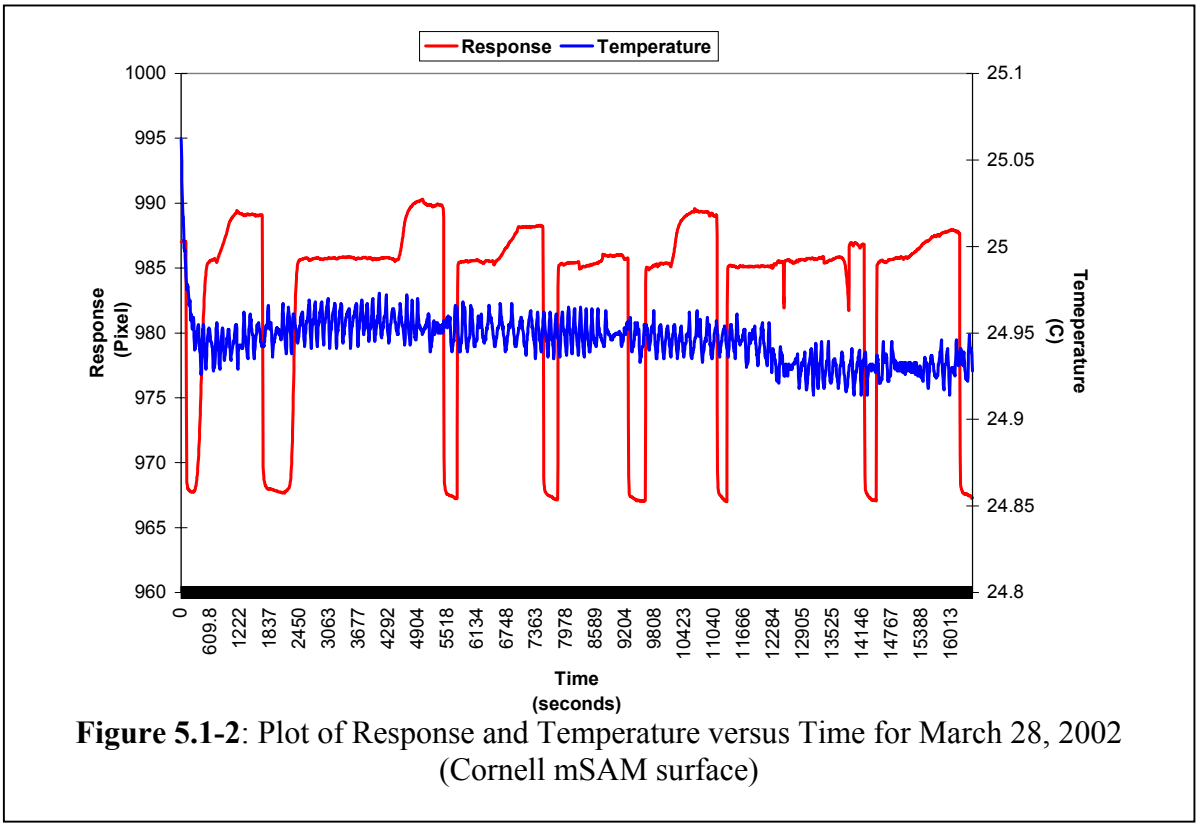

Figure 5.1-2: Plot of Response and Temperature versus Time for March 28, 2002 (Cornell mSAM surface)

5.2 Solutions used for SPR Experiments

Three solutions were used for the SPR experiments: phosphate buffered saline with Tween, 20 mM sodium hydroxide (NaOH) and 20 mM sodium acetate buffer. Phosphate buffered saline with 0.005% Tween (PBST) pH 7.4 was purchased from Sigma-Aldrich Corp. (St. Louis, MO) in powder form and brought up into 1 L of deionized water according to the package directions. The solution was filtered using a bottle top filter and degassed under vacuum. The solution was then divided into two 500 ml portions and the pH of one aliquot was lowered to 5.8 with 1 N hydrochloric acid (Fisher Scientific, Pittsburgh, PA). PBST was used instead of HEPES-buffered salt solution in these experiments to reduce the amount of components used in the system. This prevents clogged tubing from high amounts of salt and refractive index changes due to slight changes in solution from different batches. The 20 mM NaOH was made by dissolving crystalline NaOH (Fisher Scientific, Pittsburgh, PA) in DI H_2O. The sodium acetate buffer for immobilization was made by starting with 0.02 M acetic acid and increasing pH to 5.47 as described in Chapter 3.

5.3 Sensor chips

Two types of planar surfaces were used for these experiments, the XanTec CP sensor chip and a planar sensor chip made at Cornell. The XanTec CP sensor chip consists of a planar carboxylated layer on the gold surface. This slide is commercially available from XanTec bioanalytics (Muenster, Germany). The Cornell chip consists of a mixed self assembled monolayer (mSAM) on the gold surface similar to the surfaces used for SPR experiments by Lahiri, Isaacs et al. (1999). Two compounds were used for the mSAM: a tri(ethylene glycol)-terminated thiol (compound 1) and a carboxylic acid-terminated thiol (compound 2). Compounds 1 and 2 were synthesized at Toronto Research Chemicals (Toronto, Canada). For the slide preparation, a mixture of 90% compound 1 and 10% compound 2 was used. The slides were prepared by Christine Campagnola and Dr. Changcheng Zhu of Professor Carl Batts' laboratory at Cornell University in Ithica, NY using a procedure similar to the procedure detailed in Lahiri, Isaacs et al (1999) (Ryan, Personal Communication). The surface presents free carboxyl groups for amine coupling and polyethylene glycol to minimize non-specific binding (Ryan, Personal Communication). Characterization of the surface is described in Lahiri, Isaacs et al. (1999).

5.4 Activation of Surfaces and Immobilization of IGF-I

The surface was activated using a solution of 0.2 M EDC and 0.05 M NHS. The solution was placed onto the chip and left there to react for 12 minutes at room temperature. Next, the chip was rinsed with 20 mM sodium acetate pH 5.47 to remove any remaining EDC/NHS. The IGF-I was then immobilized by placing a 200 μl of 0.0125 μg IGF-I/μl sodium acetate solution onto the surface of the slide and allowing it to react overnight in a container sealed under nitrogen at 4 C. IGF-I was immobilized instead of IGFBP-3 because using the larger protein as the analyte provided a larger response from the instrument and could assist with signal to noise issues. The next day, the surface was washed with deionized water. The slide was rinsed with 1 M ethanolamine and then deactivated by placing 200 μl of ethanolamine on the surface for 10 minutes at room temperature. The surface was then washed several times with deionized water to remove the ethanolamine. After washing, the slide was dried with a nitrogen hose. The slide was then coupled to the prism using the procedure described in Chapter 3.

5.5 Kinetic Experiments with IGFBP-3

5.5.1 Description of Experiments

The kinetic measurements were performed as described in chapter three with a few key differences that are detailed here. In this case, IGFBP-3 was used as the analyte instead of IGF-I. For each data set, five concentrations of IGFBP-3 were used: 20 nM, 10 nM, 5 nM, 2.5 nM and 1.25 nM. In these experiments, 20 mM NaOH was used for regeneration of the sensor surface. We chose to use a strong base instead of the 10 mM HCl used in the previous experiments because we found that IGFBP-3 was still bound to the surface after hydrochloric acid regeneration.

5.5.2 Results of Kinetic Experiments

5.5.2-1 XanTec CP Sensor Chip

Using a XanTec CP sensor chip, the pixel response during the IGFBP-3 association phase at pH 7.4 increased with time and the highest concentration reached the highest peak value. In the dissociation phase, little to no dissociation of the IGFBP-3 from the immobilized IGF-I during the time frame of our experiment was evident. This does not agree with the expected exponential decay for a 1:1 binding model. Data for experiments run at pH 5.8 was similar (not shown).

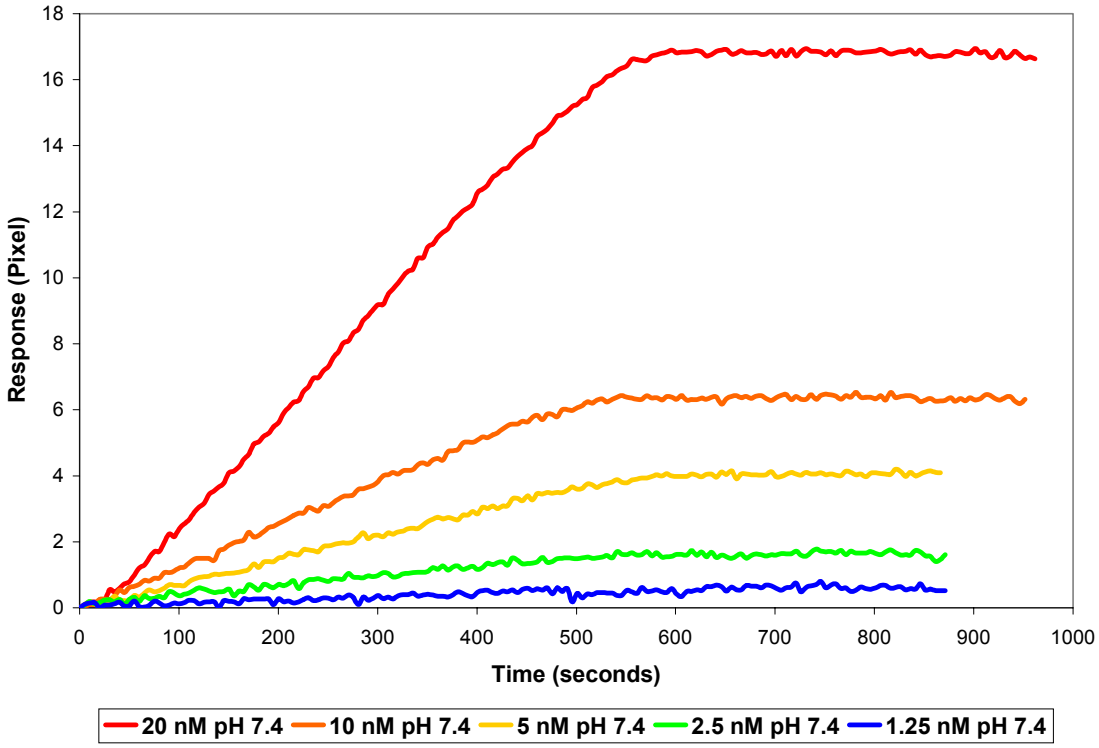

Figure 5.5.2-1: Results from an experiment at pH 7.4 using a XanTec CP sensor chip
Dissociation phase begins at time equals 480 seconds

5.5.2-2 Cornell mSAM Chip

In a similar way, a rise in pixel response was seen during the IGFBP-3 association phase with the highest peak value reached with the highest IGFBP-3 concentration (Figure 5.5.2-2). In the dissociation phase, a slight decrease with time that flattens out after approximately 50 seconds of dissociation was evident indicating little to no dissociation within the time frame of our experiment. The data looks similar for experiments run at pH 5.8 (not shown). The Cornell Chip gave a significantly lower peak height (6 pixels for 20 nM IGFBP-3) than the XanTec surface (17 pixels for 20 nM IGFBP-3) indicating that there was more IGF-I immobilized on the XanTec surface.

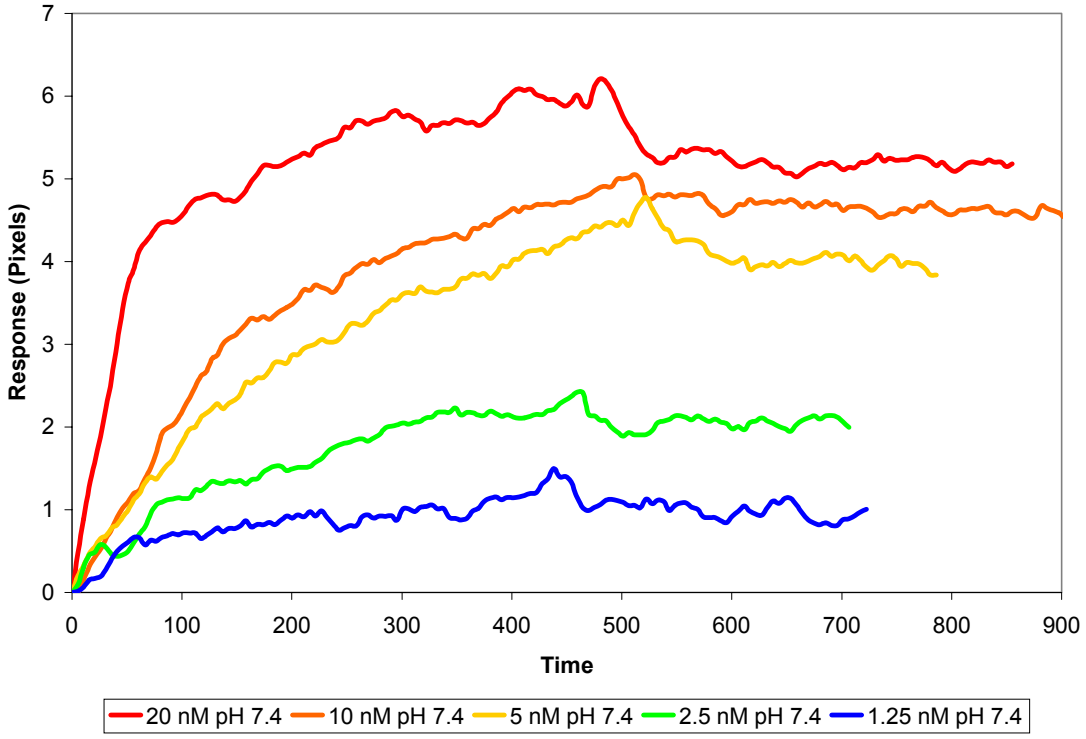

Figure 5.5.2-2: Results from an experiment at pH 7.4 using a Cornell sensor chip The dissociation phase begins at time equals 480 seconds.

5.5.3 Data Analysis

5.5.3-1 XanTec CP Sensor Chip

Data was fit to the one-site model described in Chapter 2. Graph Pad Prism software (GraphPad Software, San Diego California USA, www.graphpad.com, Version 3.02 (trial), April 25, 2000) was used for fitting the data. The association data fit well to this model as indicated by R^2 values close to 1 and no visible patterns in the residual data (figure 5.5.3-1). For each concentration, two parameters, Y_{max} and k_{obs}, were obtained. Plotting k_{obs} versus concentration should yield a straight line with the slope equal to the association rate constant as described in the literature review (Chapter 2). For these experiments, even though the association data fit extremely well to the one-site rapid mixing model, the plots of k_{obs} versus concentration did not yield a straight line (figure 5.5.3-2). The k_{obs} values decrease with increasing concentration. We feel that this may reflect a more complicated phenomenon occurring at the sensor surface.

A

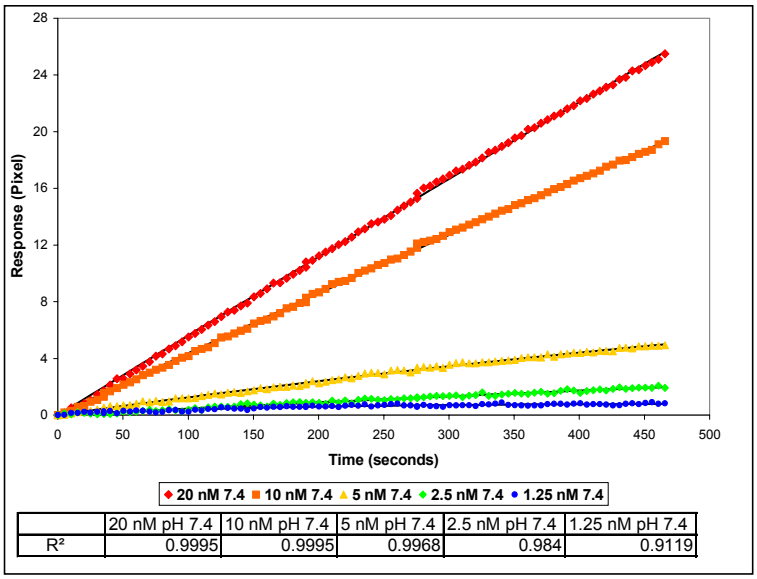

	20 nM pH 7.4	10 nM pH 7.4	5 nM pH 7.4	2.5 nM pH 7.4	1.25 nM pH 7.4
R^2	0.9995	0.9995	0.9968	0.984	0.9119

B

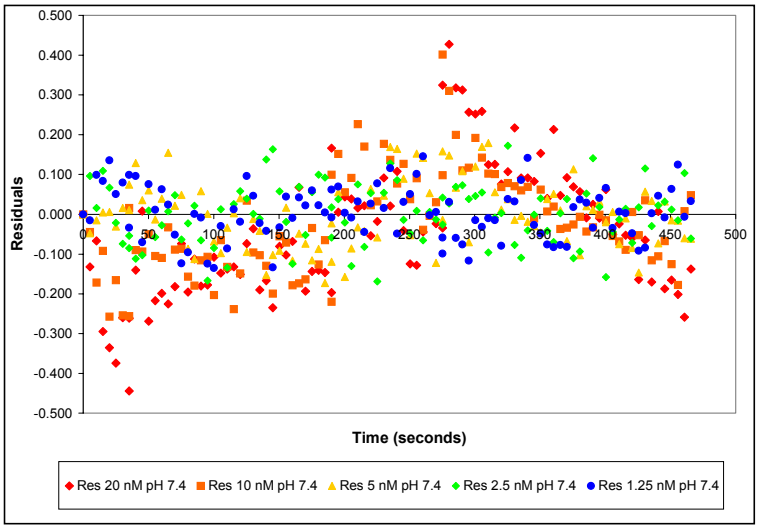

Figure 5.5.3-1: Fit with One-site Model – XanTec CP **A**: Fit of association data with one-site model – XanTec surface **B**: Residuals on fit of association data in A

Because of the non-linear k_{obs} versus concentration plots kinetic constants could not be determined for data obtained using this surface.

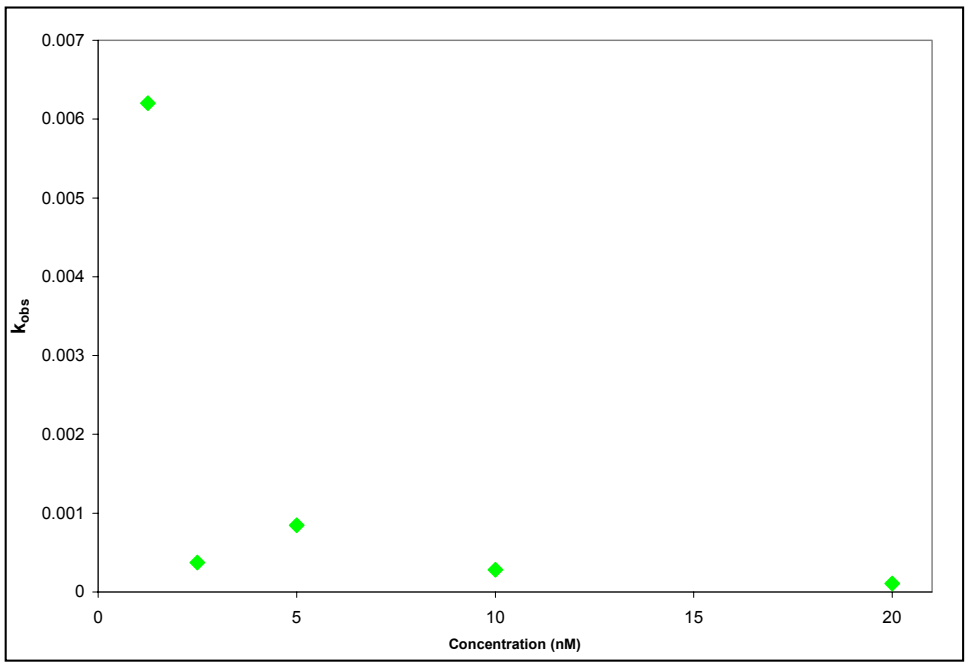

Figure 5.5.3-2: Plot of k_{obs} versus concentration for XanTec chip data – Data does not exhibit a linear pattern of increasing k_{obs} with increasing concentration

The dissociation data did not fit well to the one-site model. The data does not appear to decay exponentially toward zero as expected for the one-site model. In fact, the data appears to be a horizontal line indicating no dissociation within the time frame of our experiment. The residuals also show a distinct pattern when the data is fit to the one-site model (not shown). As a result the dissociation rate constants could not be obtained from this data set.

5.5.3-2 Cornell mSAM Chip

Association data from the Cornell mSAM surfaces was fit to the rapid mixing model as well. This data fit fairly well to this model. The R^2 values are very close to one and the residuals fall between –0.6 and 0.6. The residuals do show a slight pattern, however, this is most likely due to slight variations from noise in the instrument. Three sets of data with five concentrations of IGFBP-3 were obtained for each pH level. The association constants were obtained by plotting k_{obs} versus concentration as described in the literature review in Chapter 2 (Figure 5.5.3-3). Table 5.5.3-1 shows the association constants for each experiment and the average constant for each pH with the standard deviations. A one-way ANOVA was performed

on the values in this table using SAS (SAS Institute Inc., Cary, NC, Release 8.2). The association constants for the two pH levels are not significantly different at alpha = 0.05 (p-value = 0.2326). Increasing the number of replicates for this experiment would increase the statistical power of the test. This may help to determine if the values at the two pH levels are significantly different.

A

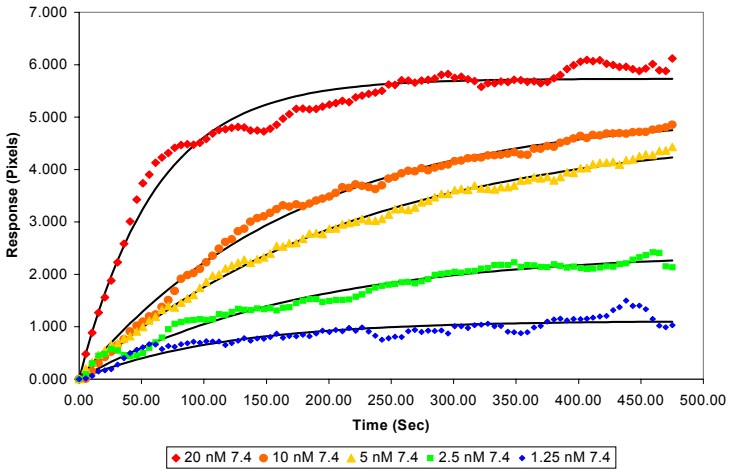

Conc.	20 nM	10 nM	5 nM	2.5 nM	1.25 nM
R^2	0.968	0.994	0.996	0.973	0.832

B

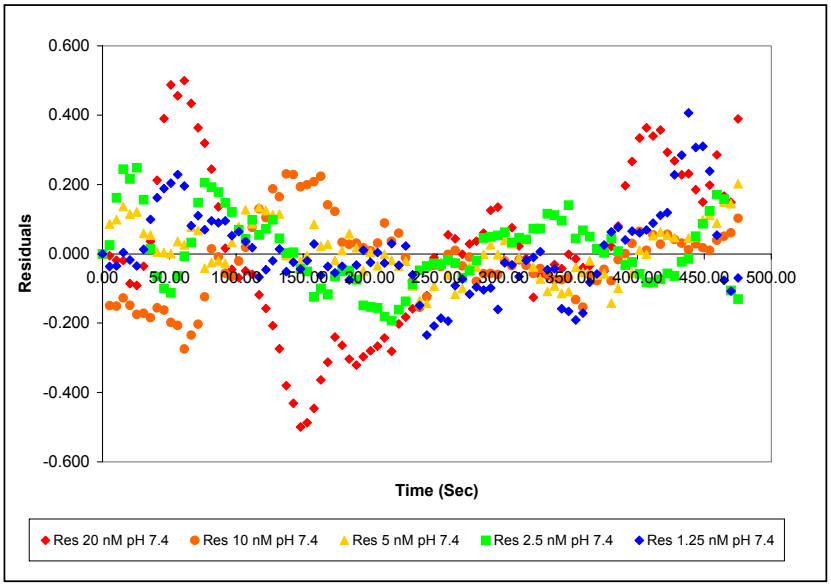

Figure 5.5.3-3: Fit with One-site Model – Cornell mSAM **A**: Fit of association data with one-site model – Cornell Surface **B**: Residuals on fit of association data

Table 5.5.3-1: Association Rate Constants from Data Obtained Using the Leica SPR 2001 Alpha (Cornell mSAM chip)

	k_a pH 5.8 (nM^{-1} s^{-1})	k_a pH 7.4 (nM^{-1} s^{-1})
March 26, 2002	7.00E-04	3.00E-04
March 27, 2002	1.00E-03	5.00E-04
March 28, 2002	3.00E-04	3.00E-04
Average	6.67E-04	3.67E-04
Std. Deviation	3.51E-04	1.15E-04

The dissociation data does not appear to decay exponentially toward zero as expected for the one-site model. The data decreases slightly but then plateaus after approximately 100 seconds. However, if the first 100 seconds of the dissociation is fit to the one-site model some of the data gives a good fit particularly at the highest analyte concentration (Figure 5.5.3-4). Longer time points appear to reflect rebinding of the analyte to the ligand. Since the association is fast, once an analyte molecule dissociates from a ligand molecule it quickly binds to another ligand molecule or to the same ligand molecule. This is seen at low analyte concentrations where the surface is not saturated with IGFBP-3 and there are many free binding sites. The lower concentrations do not fit well to the one-site model. When the first 100 seconds of the dissociation for a low analyte concentration is fit to the one-site model the data appears flat and the curve fit often increases exponentially instead of decreasing (Figure 5.5.3-5). Because some of the association data fit to the one-site model, we were able to obtain dissociation constants. At both pH 7.4 and pH 5.8, the dissociation constant is approximately 0.001 s^{-1} however there are large fluctuations between the values that are likely due to noise in the instrument. Because of these fluctuations, the dissociation constants could not be obtained reliably from this data.

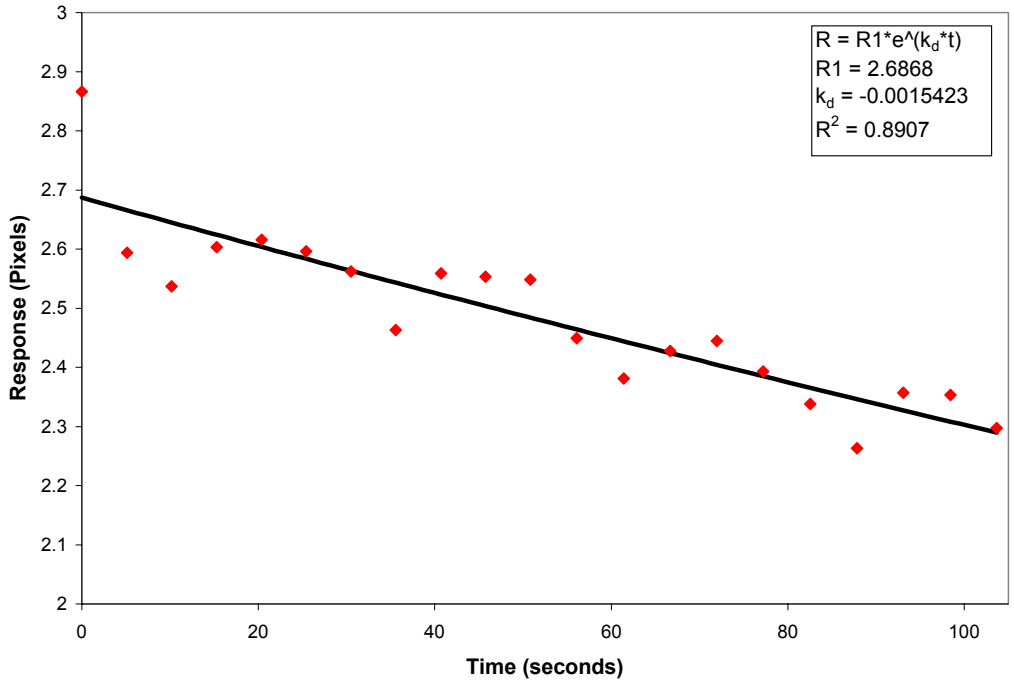

Figure 5.5.3-4: First 100 seconds of dissociation data for 20 nM IGFBP-3 at pH 7.4. Red diamonds show the data and the black line shows the fit to the one-site model. Model parameters and R^2 value are listed in the top right corner.

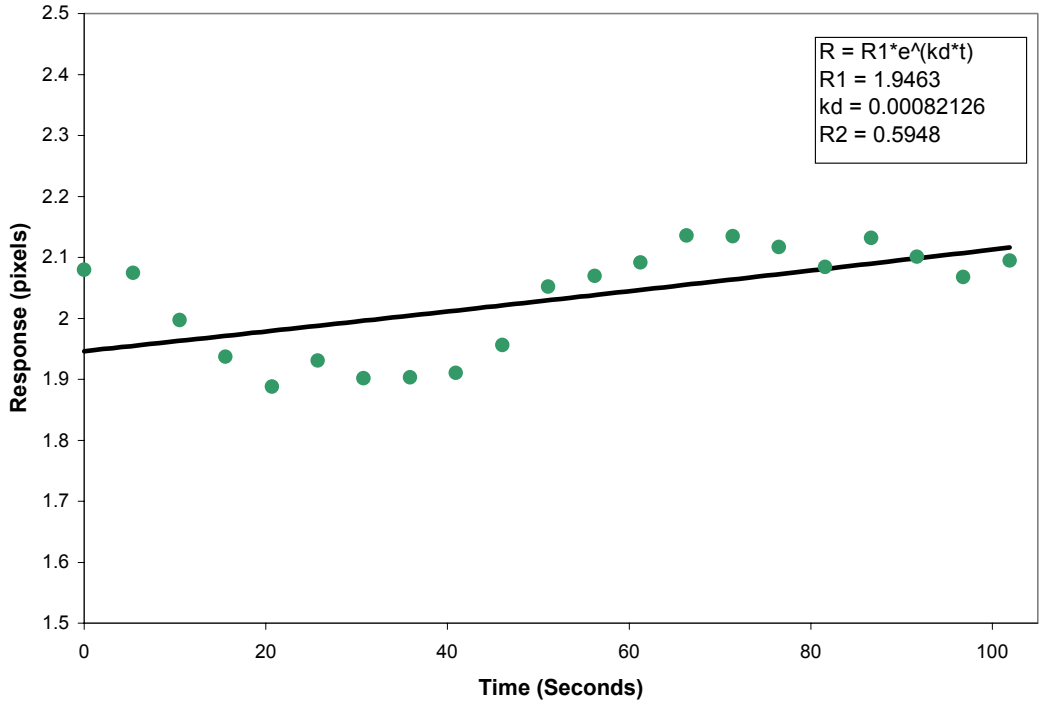

Figure 5.5.3-5: First 100 seconds of dissociation data for 2.5 nM IGFBP-3 at pH 7.4. Green circles show the data and the black line shows the fit to the one-site model. Model parameters and R^2 value are listed in the top right corner.

5.6 Summary

Two different planar carboxylated surfaces were used for immobilizing IGF-I; a XanTec CP sensor chip and a mixed self-assembled monolayer made at Cornell. In these experiments IGFBP-3 was used as the analyte. The association data from the XanTec chip fit well to the one-site model. However when plots of the observed kinetic constant, k_{obs}, versus concentration were made the plots were not linear. The dissociation data did not fit the exponential dissociation equation expected for the one-site model. These data appeared as a nearly horizontal line that did not decay toward zero as expected. Consequently, kinetic parameters could not be obtained from the XanTec chip. The association data obtained from the Cornell chip were fit well by the one-site model. Association constants for each pH level were obtained from the Cornell chip but were not significantly different. Increasing the number of replicates will increase the power of the statistical test and may show a significant difference between the rate constants. The first 100 seconds of the dissociation fit fairly well to the one-site model, particularly at the highest analyte concentration. The plateau of the dissociation at later times is likely due to rebinding because of the fast association kinetics. This is seen particularly well at low analyte concentrations where the surface is not saturated with IGFBP-3. The dissociation rate constant could not be obtained this surface due to high fluctuations in the values obtained. These fluctuations are probably due to noise in the instrument. Alternative techniques may be necessary (equilibrium analysis on SPR or via charcoal assay) to find the dissociation constants.

5.7 Future Work

Since the Cornell chip gave association data that was fit well by the one-site model repeating the experiments performed will give more samples for comparison. The greater statistical precision obtained by having more samples may lead to significantly different association rate constants. We are planning to repeat the experiment several times to obtain more association data using the Leica SPR 2001 Alpha. Since the dissociation constants could not be determined from this data, we plan to obtain the equilibrium dissociation constant, K_d, which equals k_d/k_a to obtain values for the dissociation rate constants at each pH. The equilibrium dissociation constant will be obtained from SPR experiments where the system is allowed to reach equilibrium in the association phase. Data fitting methods for this type of experiment are found in the BIAtechnology Handbook (1994). Additionally, Leica Microsystems

anticipates having modifications to the system completed which will further increase the signal to noise ratio. This may allow us to obtain the dissociation constants directly from the dissociation data. Since the lack of dissociation may be a function of the proteins used or an artifact caused by the use of the mSAM surface, we plan to use an antibody for IGF-I that binds weakly to IGF-I to see if this will dissociate from the immobilized IGF-I. We would also like to run an experiment with a protein that does not bind to IGF-I as a negative control. Finally, to test if the rate constants obtained are a function of the protein immobilized, we plan to run a series of experiments where IGFBP-3 is immobilized and IGF-I is the analyte.

Chapter 6 – Summary and Future Work

6.0 Overview of the Chapter

This chapter will summarize the studies performed for this thesis and suggest future work to accomplish our ultimate research goals. Specifically, it will summarize the initial experiments on the Leica Bio-SPR 9000 at Virginia Tech and conclusions drawn from these studies. Next, it will describe the work performed on a BIAcore 2000 instrument available to us through Douglas Lauffenburger at MIT and the conclusions drawn from those experiments. Then the chapter will discuss the experiments performed on the Leica SPR 2001 Alpha system at Leica Microsystems Analytical and Educational Services Division in Buffalo, NY. The chapter concludes with recommendations for future work.

6.1 Leica Bio-SPR 9000 Studies

Several experiments were performed using the Leica Bio-SPR 9000. Briefly, these experiments included preliminary trials to determine if a difference in the binding at pH 7.4 and pH 5.8 was evident and several initial kinetic experiments aimed at determining the association and dissociation rate constants. The results from the kinetic experiments showed the expected trends with the peak height and slope being higher for higher concentrations in the association phase of the experiment. The data was fit to the one-site model and fit fairly well based on the R^2 values and the residual plots. Kinetic association and dissociation constants were obtained from these experiments however the association and dissociation constants could not be determined with this instrument due to the large variability between the results from the experiments.

While this was surprising, the real issue arose from our analysis of the fit. The residuals from these fits showed a definite pattern indicating model mismatch and that there may still be mass transport effects in our system. Unfortunately, using a lower surface loading to reduce these effects would likely make the signal to noise ratio too low to distinguish the SPR signal from the noise. Using an instrument with a higher signal to noise ratio might allow us to determine these constants more accurately. Consequently, we decided to investigate our system using a BIAcore 2000 instrument available to us at MIT through Professor Douglas A. Lauffenburger. We felt that the increased control over the flow rate and higher signal to noise

ratio of the BIAcore 2000 instrument might allow us to make the desired measurements and would allow us to duplicate the experimental conditions found in Heding et al. (1996).

6.2 BIAcore 2000 Studies

A BIAcore 2000 instrument available to us at MIT through Dr. Douglas A. Lauffenburger was used for several studies in an attempt to obtain the association and dissociation rate constants at the two pH levels. This instrument was used to try to reduce the variability in the kinetic constants found using the Leica Bio-SPR 9000. The data obtained from these studies was fit to the one-site, the two-site and the two-compartment models. The fits of the data to all these models showed evidence of model mismatch based on the R^2 values and the residual plots. We determined that either a more complicated model would be needed to obtain kinetic rate constants from this data or an altered experimental protocol would be needed to obtain data that met the assumptions of the one-site model.

Since a more complex model would be difficult to develop without more knowledge of what was occurring on the sensor surface, we decided that an altered experimental protocol should be used to help determine the kinetic rate constants. Specifically, we identified that a higher flow rate, a lower surface loading of ligand, and lower analyte concentrations would be needed. In addition, the thick carboxymethyl dextran layer used in the BIAcore® 2000 and Leica Bio-SPR 9000 experiments may cause additional mass transport issues and that by using a self-assembled monolayer planar surface we might be able to eliminate mass transport inherent within the dextran gel. We decided to try experiments with the altered experimental protocol on Leica Microsystems new SPR 2001 Alpha since it allowed use of a planar surface and had a higher signal to noise ratio than the Leica Bio-SPR 9000. It should be noted that since this time, we have found work in which a Biacore machine was used with a retrofit planar surface chip (Fong, Wong et al. 2002).

6.3 Leica SPR 2001 Alpha Studies

A Leica SPR 2001 Alpha was available for use through Thomas E. Ryan at Leica Microsystems Inc. Analytical and Educational Services Division in Buffalo, NY. For the studies with the Leica SPR 2001 Alpha instrument, two different planar carboxylated surfaces were used for immobilizing IGF-I: a XanTec CP sensor chip and a mixed self-assembled monolayer made

at Cornell. We chose to immobilize the IGF-I because using IGFBP-3 as the analyte would produce a larger response by the instrument during the kinetic experiments.

The individual concentration association data from the XanTec chip fit well to the one-site model, however, when plots of the observed kinetic constant, k_{obs}, versus concentration were made, the plots were not linear. The value of k_{obs} decreased with increasing concentration, which is the opposite of what is expected for the one-site model. The dissociation data did not fit the exponential dissociation equation expected for the one-site model. This data appeared as a nearly horizontal line that did not decay toward zero as expected. Consequently, kinetic parameters could not be obtained from the XanTec chip.

The one-site model, based on the R^2 values and the residual plots, fit the association data obtained from the Cornell chip fairly well. Association constants for each pH level were obtained from the Cornell chip but were not significantly different (p-value = 0.2326 from one-way ANOVA). Increasing the number of replicates will increase the power of the statistical test and may help show a significant difference between the rate constants. Our data compares well with the data from the literature sources reviewed in Chapter 2 except for the values from Fong, Wong et al. (2002) (Table 6.3-1). The values from Fong et al. are an order of magnitude larger and smaller than the values obtained in our experiments and the values from the other literature sources. The first 100 seconds of the dissociation fit fairly well to the one-site model particularly at the highest analyte concentration. The plateau of the dissociation at later times is likely due to rebinding because of the fast association kinetics. This is seen particularly well at low analyte concentrations where the surface is not saturated with IGFBP-3. The dissociation rate constant could not be obtained this surface due to high fluctuations in the values obtained. These fluctuations are likely due to noise in the instrument. Alternative techniques may be necessary (equilibrium analysis on SPR or via charcoal assay) to find the dissociation constants. The dissociation constants were not obtained in our experiments but the dissociation curves we obtained are visually similar to the curves in the literature papers. Namely, the papers reviewed in chapter 2 all present results where the dissociation decreases initially and then plateaus after a short time period. Further studies are needed using this equipment to determine if the association and dissociation rate constants are different at pH 7.4 and pH 5.8.

Table 6.3-1: Comparison of association constants from literature and our experiments

Source	k_a (M^{-1} s^{-1})
Heding et al (1996)	$3.5 \mp 0.37 \times 10^5$
Wong et al (1999)	$9.12 \mp 1.65 \times 10^5$
Dubaquie and Lowman (1999)	$3.2 \mp 0.5 \times 10^5$
Galanis et al (2001)	1.1×10^{-5}
Fong et al (2002)	$0.73 \mp 0.02 \times 10^5$
Fong et al (2002)	$21.6 \mp 0.56 \times 10^5$
Vorwerk et al (2002)	$7.87 \mp 1.00 \times 10^5$
Leica SPR 2001 Alpha pH 7.4	$3.67 \mp 1.15 \times 10^5$
Leica SPR 2001 Alpha pH 5.8	$6.67 \mp 3.51 \times 10^5$

6.4 Future Work

Several issues still need to be addressed in order to fully characterize our system and meet the goal of quantitatively measuring the binding rate constants for IGF-I and IGFBP-3 interaction. Increased statistical precision is needed to determine if there is a difference between the association constants at the two pH levels. Second, more work is needed to obtain meaningful dissociation data and to determine if the lack of dissociation seen in our experiments is an artifact of the use of the planar surface. A negative control that does not bind to IGF-I is needed to show that the response seen in our experiments is due to binding of IGFBP-3 to the immobilized IGF-I. Finally, it has been suggested that the rate constants are a function of the protein immobilized when using a dextran surface and we would like to determine if the rate constants are a function of the protein immobilized when the mSAM surface is used.

Future studies will be performed using the Leica SPR 2001 Alpha instrument because we feel that the instrument performed well in our previous experiments and we have the ability to use the planar surfaces with this instrument. We plan to repeat our previous studies from the SPR 2001 Alpha using only Cornell slides. Since the Cornell chip gave association data that was fit well by the one-site model repeating the experiments on this surface should give data the fits

well to the one-site model. For these new experiments we plan to run 6 different concentrations (2.5, 5, 10, 15, 20, 15 nM) at each pH. We feel that using more concentrations will give us more confidence in the fits of k_{obs} versus concentration and therefore more confidence in the association rate constants obtained. We also plan to repeat the experiments on 3 separate surfaces. Since the surfaces can be saved overnight for use on a subsequent day we will be able to perform two experiments per surface giving a total of six experiments of six concentrations at each pH. This should help to increase our statistical precision and allow differences in the rate constants to be demonstrated.

Since the dissociation constants could not clearly be determined from this data we obtained, we plan to obtain the equilibrium dissociation constant, K_D, which equals k_d/k_a to obtain values for the dissociation rate constants at each pH. The equilibrium dissociation constant will be obtained from SPR experiments where the system is allowed to reach equilibrium in the association phase. A solution binding charcoal assay will also be performed and the equilibrium dissociation constant obtained from the charcoal assay will be compared with the results from the equilibrium SPR experiment.

The new studies will also include two control experiments. The first control experiment will use a molecule that will dissociate from IGF-I such as an antibody to demonstrate that the lack of dissociation is due to the slow dissociation rate of IGFBP-3 from IGF-I and not an artifact of the planar surface. The second control experiment will use a molecule that does not bind to IGF-I as a negative control.

To test if the rate constants obtained are a function of the protein immobilized, we plan to run a series of experiments where IGFBP-3 is immobilized and IGF-I is the analyte. Fong et al (2002) suggest that on the carboxymethyl dextran surface the rate constants depend on the protein immobilized and we would like to see if this is the case for the mSAM surface. For the previous experiments, pH 7.4 experiments were always run before pH 5.8 experiments. In our future studies, we plan to randomize the order that the pH levels are run in along with our randomization of the order of the concentrations. Finally, to obtain a value for R_{max}, the total

number of binding sites on the surface, we plan to perform a large analyte injection to completely saturate the surface, which will allow the determination of this value.

References

Arai, T., A. Parker, et al. (1994). "Heparin, heparan sulfate, and dermatan sulfate regulate formation of the insulin-like growth factor-I and insulin-like growth factor-binding protein complexes." J Biol Chem **269**(32): 20388-93.

Bach, L. A. and M. M. Rechler (1996). "Measurement of insulin-like growth factor (IGF)-II binding to purified IGF binding proteins 1-6: comparison of charcoal adsorption and high performance size exclusion chromatography." Biochim Biophys Acta **1313**(1): 79-88.

Biacore AB (1996). BIACore 2000 Product Information. Uppsala, Sweden, Biacore AB. Product Information

Biacore AB (1999). Amine Coupling Kit Instructions for Use. Uppsala, Sweden, Biacore AB. Product Instructions

Biacore AB (2002). Biacore Webpage. http://www.biacore.com Accessed: March 15, 2002

Chakkalakal, D. A., A. A. Mashoof, et al. (1994). "Mineralization and pH relationship in healing skeletal defects grafted with demineralized bone matrix." J Biomed Mater Res **28**(12): 1439-43.

Clemmons, D. R., W. Busby, et al. (1998). "Modifications of insulin-like growth factor binding proteins and their role in controlling IGF actions." Endocr J **45 Suppl**: S1-8.

Clemmons, D. R., M. L. Dehoff, et al. (1992). "Competition for binding to insulin-like growth factor (IGF) binding protein-2, 3, 4, and 5 by the IGFs and IGF analogs." Endocrinology **131**(2): 890-5.

Collett-Solberg, P. F. and P. Cohen (2000). "Genetics, chemistry, and function of the IGF/IGFBP system." Endocrine **12**(2): 121-36.

Conover, C. A. (1992). "Potentiation of insulin-like growth factor (IGF) action by IGF-binding protein-3: studies of underlying mechanism." Endocrinology **130**(6): 3191-9.

DeMellow, J. S. M. and R. C. Baxter (1988). "Growth Hormone-Dependent Insulin-like Growth Factor (IGF) Binding Protein Both Inhibits and Potentiates IGF-I Stimulated DNA Synthesis in Human Skin Fibroblasts." Biochemical and Biophysical Research Communications **156**(1): 199-204.

Dessy, R. (2002). Professor Emeritus, Virginia Polytechnic Institute and State University. Personal Communication

Dubaquie, Y. and H. B. Lowman (1999). "Total alanine-scanning mutagenesis of insulin-like growth factor I (IGF-I) identifies differential binding epitopes for IGFBP-1 and IGFBP-3." Biochemistry **38**(20): 6386-96.

Earp, R. L., and Raymond E. Dessy (1998). Surface Plasmon Resonance. Commercial Biosensors: Applications to Clinical, Bioprocess, and Environmental Samples. G. Ramsay, John Wiley & Sons, Inc.**:** 99-164.

Edwards, P. R., C. H. Maule, et al. (1998). "Second-order kinetic analysis of IAsys biosensor data: its use and applicability." Anal Biochem **263**(1): 1-12.

Ferry, R. J., Jr., L. E. Katz, et al. (1999). "Cellular actions of insulin-like growth factor binding proteins." Horm Metab Res **31**(2-3): 192-202.

Firth, S. M., U. Ganeshprasad, et al. (1998). "Structural determinants of ligand and cell surface binding of insulin-like growth factor-binding protein-3." J Biol Chem **273**(5): 2631-8.

Fong, C. C., M. S. Wong, et al. (2002). "Effect of hydrogel matrix on binding kinetics of protein-protein interactions on sensor surface." Analytica Chimica Acta **456**(2): 201-208.

Forsten, K. E., R. M. Akers, et al. (2001). "Insulin-like growth factor (IGF) binding protein-3 regulation of IGF-I is altered in an acidic extracellular environment." J Cell Physiol **189**(3): 356-65.

Galanis, M., S. M. Firth, et al. (2001). "Ligand-binding characteristics of recombinant amino- and carboxyl-terminal fragments of human insulin-like growth factor-binding protein-3." J Endocrinol **169**(1): 123-33.

Geduspan, J. S. and M. Solursh (1993). "Effects of the mesonephros and insulin-like growth factor I on chondrogenesis of limb explants." Dev Biol **156**(2): 500-8.

Heding, A., R. Gill, et al. (1996). "Biosensor measurement of the binding of insulin-like growth factors I and II and their analogues to the insulin-like growth factor-binding protein-3." J Biol Chem **271**(24): 13948-52.

Horan, N., L. Yan, et al. (1999). "Nonstatistical binding of a protein to clustered carbohydrates." Proc Natl Acad Sci U S A **96**(21): 11782-6.

Jansson, M., J. Dixelius, et al. (1997). "Binding affinities of insulin-like growth factor-I (IGF-I) fusion proteins to IGF binding protein 1 and IGF-I receptor are not correlated with mitogenic activity." FEBS Lett **416**(3): 259-64.

Johnsson, B., S. Lofas, et al. (1991). "Immobilization of proteins to a carboxymethyldextran-modified gold surface for biospecific interaction analysis in surface plasmon resonance sensors." Anal Biochem **198**(2): 268-77.

Jones, J. I. and D. R. Clemmons (1995). "Insulin-like growth factors and their binding proteins: biological actions." Endocr Rev **16**(1): 3-34.

Karas, M., M. Danilenko, et al. (1997). "Membrane-associated insulin-like growth factor-binding protein-3 inhibits insulin-like growth factor-I-induced insulin-like growth factor-I receptor signaling in ishikawa endometrial cancer cells." J Biol Chem **272**(26): 16514-20.

Kiefer, M. C., C. Schmid, et al. (1992). "Characterization of recombinant human insulin-like growth factor binding proteins 4, 5, and 6 produced in yeast." J Biol Chem **267**(18): 12692-9.

Koedam, J. A., C. M. Hoogerbrugge, et al. (1997). "Solid-phase assay for insulin-like growth factor (IGF) binding to IGF-binding protein-3: application to the study of the effects of antibodies and heparin." J Endocrinol **153**(1): 87-97.

Lahiri, J., L. Isaacs, et al. (1999). "A strategy for the generation of surfaces presenting ligands for studies of binding based on an active ester as a common reactive intermediate: a surface plasmon resonance study." Anal Chem **71**(4): 777-90.

Marinaro, J. A., G. P. Jamieson, et al. (1999). "Differential dissociation kinetics explain the binding preference of insulin-like growth factor binding protein-6 for insulin-like growth factor-II over insulin-like growth factor-I." FEBS Lett **450**(3): 240-4.

Martin, J. L. and R. C. Baxter (1986). "Insulin-like growth factor-binding protein from human plasma. Purification and characterization." J Biol Chem **261**(19): 8754-60.

Martin, J. L., K. E. Willetts, et al. (1990). "Purification and properties of a novel insulin-like growth factor-II binding protein from transformed human fibroblasts." J Biol Chem **265**(7): 4124-30.

McCusker, R. H., W. H. Busby, et al. (1991). "Insulin-like growth factor (IGF) binding to cell monolayers is directly modulated by the addition of IGF-binding proteins." Endocrinology **129**(2): 939-49.

McCusker, R. H., C. Camacho-Hubner, et al. (1990). "Insulin-like growth factor (IGF) binding to human fibroblast and glioblastoma cells: the modulating effect of cell released IGF binding proteins (IGFBPs)." J Cell Physiol **144**(2): 244-53.

Mochizuki, H., Y. Hakeda, et al. (1992). "Insulin-like growth factor-I supports formation and activation of osteoclasts." Endocrinology **131**(3): 1075-80.

Morton, T. A. and D. G. Myszka (1998). "Kinetic analysis of macromolecular interactions using surface plasmon resonance biosensors." Methods Enzymol **295**: 268-94.

Morton, T. A., D. G. Myszka, et al. (1995). "Interpreting complex binding kinetics from optical biosensors: a comparison of analysis by linearization, the integrated rate equation, and numerical integration." Anal Biochem **227**(1): 176-85.

Muta, K. and S. B. Krantz (1993). "Apoptosis of human erythroid colony-forming cells is decreased by stem cell factor and insulin-like growth factor I as well as erythropoietin." J Cell Physiol **156**(2): 264-71.

Myszka, D. G., X. He, et al. (1998). "Extending the range of rate constants available from BIACORE: interpreting mass transport-influenced binding data." Biophys J **75**(2): 583-94.

Oh, Y., H. L. Muller, et al. (1993). "Characterization of the affinities of insulin-like growth factor (IGF)-binding proteins 1-4 for IGF-I, IGF-II, IGF-I/insulin hybrid, and IGF-I analogs." Endocrinology **132**(3): 1337-44.

Ott, R. L. and M. Longnecker (2001). An Introduction to Statistical Methods and Data Analysis. Pacific Grove, California, Duxbury.

Pahlman, S., G. Meyerson, et al. (1991). "Insulin-like growth factor I shifts from promoting cell division to potentiating maturation during neuronal differentiation." Proc Natl Acad Sci U S A **88**(22): 9994-8.

Pharmacia Biosensor AB (1994). BIAtechnology Handbook. Uppsala, Sweden, Pharmacia Biosensor AB.

Rao, J., L. Yan, et al. (1999). "Binding of a dimeric derivative of vancomycin to L-Lys-D-Ala-D-lactate in solution and at a surface." Chem Biol **6**(6): 353-9.

Rodriguez-Tarduchy, G., M. K. Collins, et al. (1992). "Insulin-like growth factor-I inhibits apoptosis in IL-3-dependent hemopoietic cells." J Immunol **149**(2): 535-40.

Roush, E. (2001). Application Specialist, BIAcore International AB. Personal Communication

Ryan, T. E. (2002). Business Director of BioAnalytical Solutions, Leica Microsystems Inc. Educational and Analytical Services Division. Personal Communication

Schuck, P. (1996). "Kinetics of ligand binding to receptor immobilized in a polymer matrix, as detected with an evanescent wave biosensor. I. A computer simulation of the influence of mass transport." Biophys J **70**(3): 1230-49.

Schuck, P. (1997). "Use of surface plasmon resonance to probe the equilibrium and dynamic aspects of interactions between biological macromolecules." Annu Rev Biophys Biomol Struct **26**: 541-66.

Schuck, P. and A. P. Minton (1996). "Analysis of mass transport-limited binding kinetics in evanescent wave biosensors." Anal Biochem **240**(2): 262-72.

Scott, C. D., J. L. Martin, et al. (1985). "Production of insulin-like growth factor I and its binding protein by adult rat hepatocytes in primary culture." Endocrinology **116**(3): 1094-101.

Spector, J. A., B. J. Mehrara, et al. (2001). “Osteoblast expression of vascular endothelial growth factor is modulated by the extracellular microenvironment.” Am J Physiol Cell Physiol **280**(1): C72-80.

Street D. B. J., Juel C (2001). “Interstitial pH in human skeletal muscle during and after dynamic graded exercise.” JOURNAL OF PHYSIOLOGY-LONDON **537**(3): 993-998.

Stubbs, M., McSheehy, P. M., et al. (2000). "Causes and consequences of tumour acidity and implications for treatment." Mol Med Today **6** (1):15-19.

Vorwerk, P., B. Hohmann, et al. (2002). “Binding properties of insulin-like growth factor binding protein-3 (IGFBP-3), IGFBP-3 N- and C-terminal fragments, and structurally related proteins mac25 and connective tissue growth factor measured using a biosensor.” Endocrinology **143**(5): 1677-85.

Werner, H. and D. LeRoith (1996). “The role of the insulin-like growth factor system in human cancer.” Adv Cancer Res **68**: 183-223.

Williams, G. T., C. A. Smith, et al. (1990). “Haemopoietic colony stimulating factors promote cell survival by suppressing apoptosis.” Nature **343**(6253): 76-9.

Wong, M. S., C. C. Fong, et al. (1999). “Biosensor measurement of the interaction kinetics between insulin-like growth factors and their binding proteins.” Biochim Biophys Acta **1432**(2): 293-301.

XanTec Bioanalytics (2002). XanTec Webpage. http://www.xantec.com
Accessed: March 1, 2002

VITA

Theresa R. Cassino

Theresa Cassino was born in Houston, Texas in 1978 to Mary and Toby Gouker. She attended Glenelg High School and upon her graduation in 1996 she moved to Glassboro, New Jersey to attend Rowan University. Theresa received numerous awards and honors during her undergraduate career including the Best Paper Award (Delaware Valley AIChE), the Donald F. Othmer Sophomore Academic Excellence Award (AIChE), the 1998 Annual Top Student Award (South Jersey AIChE), the 1997 Outstanding Engineering Student Award (PE Society of Southern NJ), and the four year PRIDE 2000 Full Tuition Scholarship. Theresa Cassino graduated from Rowan University magna cum laude in May 2000 with her Bachelors of Science in Chemical Engineering.

Upon graduation from Rowan, Theresa moved to Blacksburg, Virginia and began her graduate work at Virginia Polytechnic Institute and State University in the fall of 2000. In her first year of graduate studies Theresa was awarded a Virginia Tech General Electric Scholars Fellowship and a Virginia Tech Center for Biomedical Engineering Pratt Scholarship. In the spring of 2001 Theresa was awarded a three year National Science Foundation Graduate Fellowship. Theresa Cassino presented her masters research at the 2001 Annual AIChE meeting in Reno, NV and was awarded the Best Poster Award for the Food, Pharmaceutical and Bioengineering division. In June 2001, Theresa married Christopher Cassino, who she met at Rowan University.

Upon completion of her Masters of Science degree in June 2002, Theresa Cassino plans to begin Ph.D. studies at Virginia Tech in the Chemical Engineering Department. Her Ph.D. work will involve characterizing the effects of chemical and mechanical stimulation on equine chondrocytes.